POLITECNICO DI TORINO

Department of Control and Computer Engineering

Master of Science in Mechatronic Engineering

Master Degree Thesis

SHORT TERM SEA WAVE FORCE PREDICTION FOR FEEDBACK CONTROL OF A WAVE ENERGY CONVERTER

Surpervisors
Prof. Diego Regruto
Prof. Vito Cerone
Prof. Massimo Canale

Author
Silvia Zedda

April, 2019

Contents

List of Figures

List of Tables

Abstract

This thesis is about the design of a virtual sensor-based predictor for an offshore, single body, floating sea wave energy converter called ISWEC (Inertial Sea Wave Energy Converter). The pitch rotation of the floater, due to the incoming waves, is combined to the flywheel spinning velocity generating an inertial gyroscopic torque. The Inertial Sea Wave Energy Converter exploits the gyroscopic effect to generate energy. In order to maximize the generated energy, a model predictive control algorithm based on the prediction of future values of the pitch component of the incident wave force, has to be exploited. However, since no sensor is available on the ISWEC for measuring the pitch force, prediction of future values of such quantity is a challenging problem. In this work an original two-stages approach is proposed for the design of the wave force prediction. In the first stage a virtual sensor able to provide real-time estimation of the wave force is designed by applying the set-membership estimation theory. In the second stage, an autoregressive linear filter able to predict future values of the wave force based on the current and past values of the same quantity estimated by the virtual sensor is obtained by means of standard least squares. The designed prediction algorithm has been successfully tested on different data sets obtained from an accurate simulator of the ISWEC prototype.

Chapter 1

Introduction

Nowadays one of the threats that most impacts on worldwide choices is global warming. Solar radiations arrive on Earth in form of light waves, some of them come back into space and others are trapped by the atmosphere, making the Earth temperature remain constant.

Starting from the industrial revolution, in factories, large quantities of coal were started burning, producing the so-called greenhouse gases. Numerous scientific studies have shown that climate change is linked to the use of fossil energy sources, in fact greenhouse gases reaching the atmosphere, make it thicker so that many more rays are retained and this causes an excessive heating of the planet, as a consequence there are numerous environmental effects:

- glaciers melting
- increase in precipitation
- drying up of whole regions resulting in drought
- oceans warming resulting in powerful hurricanes

To prevent global warming from having catastrophic effects on the environment, renewable energy sources are becoming increasingly common. Renewable energy sources are those whose use does not affect future availability; Hydropower, wind turbines and solar Photo Voltaic panels are the most diffused but other sources are represented by bio-power, geothermal power, concentrating solar thermal power, wind power and ocean power. In 2016, in UE, among the renewable sources the main ones were wood and other solid biofuels, hydropower provided the second largest contributor to the renewable energy followed by wind energy. Very low quantities of tidal, oceanic and wave energy have been produced; these technologies are used mainly in France and United Kingdom. [1] Among the sources, the oceanic one contains large amounts of both mechanical and thermic energy and at least five types of energy can be converted:

- Tidal Energy
- Marine Current Power
- Osmotic Power
- Ocean Thermal Energy
- Wave Energy

From now on, the focus of this thesis will be on wave energy.

1.1 Wave Energy

Waves are generated by the force of wind blowing on the surface of the sea and by exploiting the kinetic energy contained in the wave motion it is possible to produce electricity. The kinetic energy of a wave depends on speed and duration of the wind, on the depth of the water, on the conditions of the backdrop and on the interaction with the other waves. The study of wave motion is more complex than that of other renewable energy sources and for this reason the attempt to produce electrical energy from waves is quite recent. The device that allows to convert the kinetic energy of the waves into electric energy, is called Wave Energy Converter. Relatively to [2], WECs can be easily classified according to their *working principle* and *location*. Talking about the primary conversion working principle, the classification is:

- **Oscillating Water Columns (OWC)** made of a semi-submerged chamber opened at the bottom. The superior chamber is linked to the external environment through a duct in which flows the air pressurized in the chamber by the water vertical motion due to waves' action.
- **Wave Activated Bodies (WAB)** made of a single or multiple body. The mechanical energy of the buoy comes from the pressure and kinetic energy of the waves.
- **Overtopping devices** made of a storage basin, inside which the water level is higher than the sea level. The water inside the basin is returned to the sea by an hydraulic turbine.

According to its location, the device can be classified as:

- **Onshore** the device is located at the shore, this leads to low installation and maintenance costs but on the other hand it is subjected to the high power of wave during storms and generally, waves contain less energy.
- **Nearshore** the device is located in moderate water depths (from 10m to 25m).
- **Offshore** the device is located in waters of more than 40m of depth. Installation and maintenance costs are expensive but waves contain an higher energy.

This thesis is about the ISWEC, an offshore, single body, floating wave energy converter. All the following informations are derived from [2].

1.2 ISWEC

The Inertial Sea Wave Energy Converter exploit the gyroscopic effect to generate energy. It consists of a monolithic hull, two gyroscopic units, an electric PTO, a power conditioning system and an electric cable. The two gyroscopes, the PTO and the power conditioning system are located in the inner space that is completely sealed with respect to the external environment, only the electric cable crosses the hull from the inner to the outer side and thanks to the sealing, corrosion and maintenance expenses are significantly reduced. The floater mooring systems involves a slack mooring configuration composed of a single line, a jumper and a clump weight, thanks to this configuration the hull is able to align itself to the wavefront direction. The pitch rotation of the floater around the δ axis, due to the incoming waves, is combined to the flywheel spinning velocity $\dot{\psi}$, generating an inertial gyroscopic torque that makes the gyroscopic structure rotate around the precession axis ε. Electricity is produced braking the motion of the electric motor mounted on the same shaft of the gyroscopic structure. In figure, is shown the prototype and its sea installation.

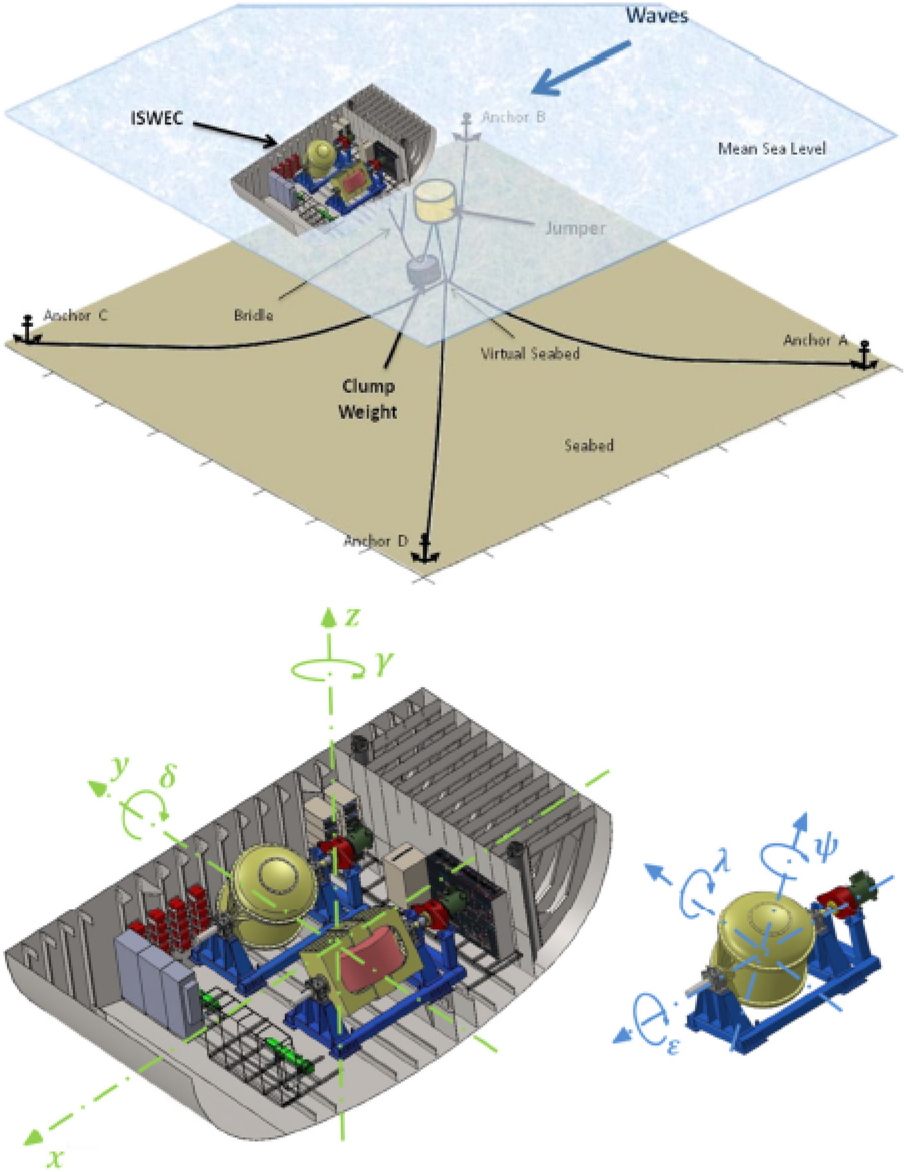

Figure 1.1: ISWEC prototype and installation [2]

1.2.1 Project

The Inertial Sea Wave Energy Converter (ISWEC) is a device designed by the Mechanical and Aerospace Engineering department of Politecnico di Torino (Italy), the first idea is dated to 2005 and was about a 2 degrees of freedom gyroscope system. In 2007, to test the possibility of converting waves' energy to electricity through the combination of the motion of a hull and a flywheel spinning speed, a 1 degree of freedom system was tested. The PTO has been installed on the same shaft of the gyroscope frame. A first ISWEC prototype was developed in 2009 to be installed in Alghero site (Sardinia, Italy), a 1:45 scaled device was used to validate the mathematical and numerical models but friction, aerodynamic losses and electric efficiency cannot be scaled so they could not be studied.

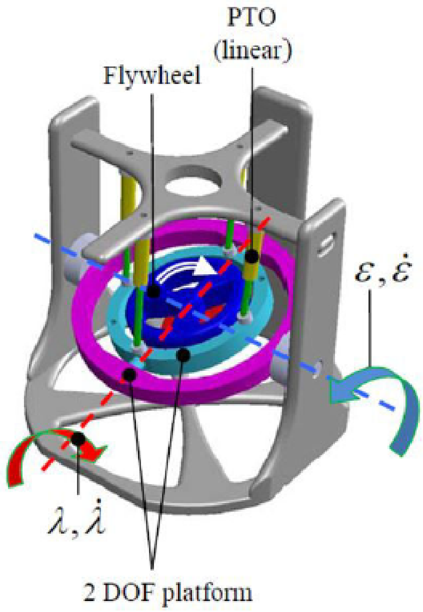

Figure 1.2: 2 Degrees of Freedom (DOF) gyroscope system [2]

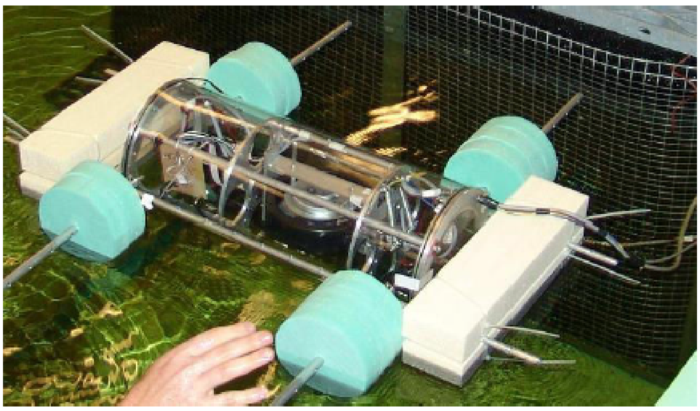

Figure 1.3: ISWEC 1:45 scaled prototype [2]

To face this problem a 1:8 scaled prototype was built and from January 2010 to December 2011, a series of waves and current measurements took place in Pantelleria site (Sicily, Italy), near the port, in the installation point of the device. Thanks to these measurements was possible to characterize the waves states in that point and more reliable simulations could be run. In 2012 the 1:8 prototype was realized and tested at INSEAN wave tank in Rome and it was installed in Pantelleria in August 2015.

1.2.2 Implementation of the ISWEC model

According to [3] the ISWEC model is implemented with the Harmonic Balance approach. The two equations describing the system are:

$$\begin{cases} (I_{eq}+\mu_\infty)\ddot{\delta}+s_w\delta+\int_0^t h(t-\tau)\dot{\delta}(\tau)d\tau+\beta|\dot{\delta}|\dot{\delta}-J_g\dot{\varphi}\dot{\varepsilon}cos(\varepsilon)-T_w=0 \\ I_g\ddot{\varepsilon}+c_{PTO}\dot{\varepsilon}+k_{PTO}\varepsilon+J_g\dot{\varphi}\dot{\delta}cos(\varepsilon)=0 \end{cases} \tag{1.1}$$

where:

- T_w torque induced on the floater by the waves
- I_{eq} momentum of inertia of the device for pitch
- μ_∞ infinite added mass
- $\int_0^t h(t-\tau)\dot{\delta}(\tau)d\tau$ convolution integral of radiation forces
- β quadratic viscous damping coefficient
- s_w linear hydrostatic stiffness
- I_g overall gyroscope momentum of inertia around the precession axis
- J_g flywheel momentum of inertia about its rotating axis
- c_{PTO} PTO damping coefficient
- k_{PTO} PTO stiffness coefficient

The first equation is related to the hull motion, the second one to the gyroscopic system. It is important to notice that the system is non-linear, due to the $J\dot{\varphi}$ term.

1.2.3 ISWEC problem formulation

Thanks to the mooring system the ISWEC works aligned to the wavefront direction and it is subject to a pitch motion, around the side-to-side axis, caused by the waves. In order to maximize the energy produced by the floater it is needed to control the PTO applying a predictive control algorithm based on the prediction of future values of the pitch force. To predict it, is required the knowledge of its value time by time but since the ISWEC has no sensor intended for measuring the pitch force applied by the waves, it can be estimated given the time measurements of the other quantities, coming from the on board sensors.
As explained above, the system is nonlinear, a possible solution is proposed in [5] and is briefly discussed in the last chapter of this thesis. The goal of this thesis is to find a simpler solution and for sake of simplicity the system from now on is considered as Linear and Time Invariant.

A standard formulation for the prediction problem is the following:

$$\widehat{y}(t+\Delta|t) = f(y(t), ..., y(t-k), u(t+\Delta), ..., u(t-h))) \tag{1.2}$$

Considering the ISWEC:

- Δ is the prediction horizon
- $\widehat{y}(t+\Delta|t)$ is the predicted Pitch Force (F_P) at time t+Δ
- y(t) is the Pitch Force (F_P) at time t
- u(t+Δ) is the future input at time t+Δ

In this specific case y(t) is unknown since it cannot be measured by any sensor on the floater while u(t) is measured but is not possible to know its future values. To deal with this two critical issues a possible solution is the two-stages approach, consisting in a first identification stage and then in a prediction stage.

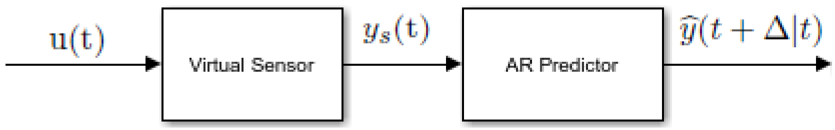

Figure 1.4: Two-stage prediction Model

1. **Virtual Sensor**
   The first stage consists of a Virtual Sensor that, given the input u(t) measured on the ISWEC, allows to estimate the Pitch Force (y_s(t)) in real time. The Virtual Sensor is designed applying the Set Membership estimation theory as discussed in the following chapter.

2. **AR Predictor**
   The second stage is an autoregressive predictor based on the following assumptions:

   - Over the prediction horizon Δ the sea state is constant;
   - At a given time the value of the Pitch Force is related to its recent past values.

   The Pitch Force can be predicted as a linear function of its past values by means of standard least squares:

$$\widehat{y}(t+\Delta|t) = \alpha_1 y_s(t) + \alpha_i y_s(t-1) + ... + \alpha_n y_s(t-n) \tag{1.3}$$

In the following chapters is discussed the result obtained applying the two-stages approach.

Chapter 2

Set-Membership Identification

2.1 System Identification

Identify a system means establish the mapping between its input and output given a set of a priori informations on the model structure. Two cases may occur:

- **Grey Box**: significant structural informations are available, based on some physical insight. It is not possible to have the exact structure of the system equation.
- **Black Box**: only bland assumptions are made on the system class.

Since in practice the problem is related to a sequence of numbers (data), even if the physical system is a continuous time system, the best thing to do is look for a discrete-time model. Consider the case of a black box, since it is the most general model.

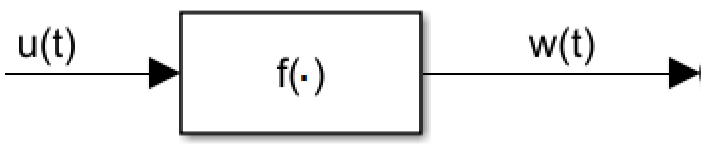

Figure 2.1: Black Box model

The purpose is that of derive a discrete-time model in the *General Regression Form* based on a set of input(u(t))/output(w(t)) discrete-time data, where t is the discrete time variable. It is assumed that in general the system is a *dynamic system*:

$$w(t) = f(w(t-1), w(t-2), ..., w(t-n), u(t), u(t-1), u(t-2), ..., u(t-m))$$

If the system is **linear** w(t) will be a linear combination of the state variables:

$$w(t) = \alpha_1 w_1(t-1) + \alpha_2 w_2(t-2) + ... + \alpha_n w(t-n) + \beta_0 u(t) + \beta_1 u(t-1) + ... + \beta_m u(t-m)$$

But if the system is **nonlinear** there are different mathematical models and *a priori assumptions* are needed: f∈F where F is the class of a function (trigonometric, polynomial, continuous, differentiable etc.). A model can be classified as:

- **Parametric** if F can be described by means of a finite number of parameters
- **Non parametric** if F cannot be described by means of a finite number of parameters

All the following considerations are based on Parametric models.

2.1.1 Noise in collected data

Input and output data are corrupted by noise, a priori informations on the noise are needed. First of all, it is possible to classify the noise structure:

1. **Equation Error (EE)**

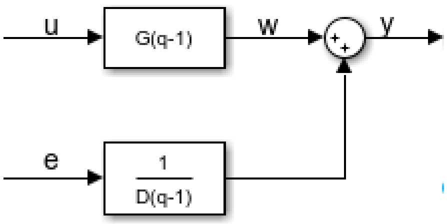

Figure 2.2: Equation Error Structure

$$D(q^{-1})y(t) = N(q^{-1})u(t) + e$$

2. **Output Error (OE)**

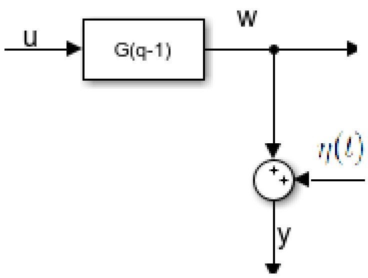

Figure 2.3: Output Error Structure

$$y(t) - \eta(t) = \frac{N(q^{-1})}{D(q^{-1})}u(t)$$

$$w(t) = y(t) - \eta(t)$$

3. **Error In Variable (EIV)**

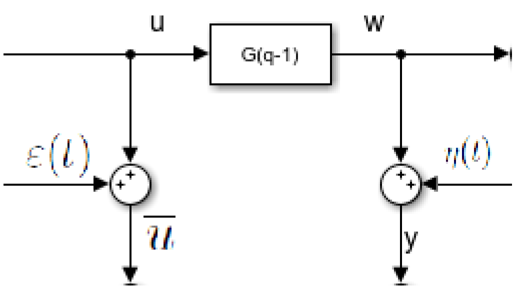

Figure 2.4: Error In Variable Structure

$$y(t) - \eta(t) = \frac{N(q^{-1})}{D(q^{-1})}(\overline{u}(t) - \varepsilon(t))$$

$$w(t) = y(t) - \eta(t)$$

$$u(t) = \overline{u}(t) - \varepsilon(t)$$

Regarding $\eta(t)$ and $\varepsilon(t)$ there are two possibilities:

- they are assumed to be random variables statistically distributed according to a probability density function which is partially known.
- they are bounded and known to belong to a given bounded set

$$|\eta(t)| \leq \Delta\eta, \forall \text{t} \quad \Delta\eta \in \Re$$
$$|\varepsilon(t)| \leq \Delta\varepsilon, \forall \text{t} \quad \Delta\varepsilon \in \Re$$

The following formulation is based on $|\eta(t)|$ and $|\varepsilon(t)|$ bounded.

2.2 Set Membership approach for system identification

Assuming a priori informations on the plant and on the noise it is possible to define the *Feasible Parameter Set.* Knowing that:

$$\text{f}\in\text{F},$$
$$(\varepsilon\text{(t)},\eta\text{(t)})\in S = \{\varepsilon(t), \eta(t) : |\eta(t)| \leq \Delta\eta, \quad |\varepsilon(t)| \leq \Delta\varepsilon, \quad t = 1, ..., N\}$$

the Feasible Parameter Set is defined as the set of all values θ which are consistent with the a-priori informations on the plant and on the noise, for all the collected data:

$$\begin{gathered} D_\theta = \{\theta = [\alpha_1, ..., \alpha_n, \beta_0, ..., \beta_n] \in \Re^{2n+1} : w(t) = -\alpha_1 w(t-1) - ... - \alpha_n w(t-n) + \beta_0 u(t) + ... + \beta_n u(t-n), \\ y(t) = w(t) + \eta(t), \quad |\eta(t)| \leq \Delta\eta, \quad \forall t = 1, ..., N, \\ \overline{u}(t) = u(t) + \varepsilon(t), \quad |\varepsilon(t)| \leq \Delta\varepsilon, \quad \forall t = 1, ..., N\} \end{gathered}$$

Since the FPS depends on the unknown samples of the noise sequences, it is needed to define the Extended Feasible Parameter Set (EFPS):

$$\begin{gathered} D_{\theta,\eta,\varepsilon} = \{\theta = [\alpha_1, ..., \alpha_n, \beta_0, ..., \beta_n] \in \Re^{2n+1}, \quad \eta = [\eta(1), ..., \eta(N)] \in \Re^N, \quad \varepsilon = [\varepsilon(1), ..., \varepsilon(N)] \in \Re^N : \\ (y(t) - \eta(t)) = -\alpha_1(y(t-1) - \eta(t-1)) - ... - \alpha_n(y(t-n) - \eta(t-n)) + \beta_0(\overline{u}(t) - \varepsilon(t))) + ... + \\ \beta_n(\overline{u}(t-n) - \varepsilon(t-n)), \quad \forall t = n+1, ..., N \\ |\eta(t)| \leq \Delta\eta, \quad \forall t = 1, ..., N, \\ |\varepsilon(t)| \leq \Delta\varepsilon, \quad \forall t = 1, ..., N\} \end{gathered}$$

The FPS has a generic non-convex shape and the Parameter Uncertainty Intervals (PUI) are defined as follow:

$$PUI = [\underline{\theta}_i, \overline{\theta}_i]$$

$$\underline{\theta}_i = \min_{\theta \in D_\theta} \theta_i \qquad \overline{\theta}_i = \max_{\theta \in D_\theta} \theta_i$$

where

$$\underline{\theta}_i = \min_{\substack{s.t. \\ y(t)=\eta(t)-\alpha_1(y(t-1)-\eta(t-1))-...-\alpha_n(y(t-n)-\eta(t-n))+\beta_0(\overline{u}(t)-\varepsilon(t)))+...+\beta_n(\overline{u}(t-n)-\varepsilon(t-n)), \quad \forall t=n+1,...,N \\ \eta(t)\leq\Delta\eta \\ \eta(t)\geq-\Delta\eta \\ \varepsilon(t)\leq\Delta\varepsilon \\ \varepsilon(t)\geq-\Delta\varepsilon, \quad \forall t=1,...,N}} \theta_i$$

and

$$\overline{\theta}_i = \max_{\substack{s.t. \\ y(t)=\eta(t)-\alpha_1(y(t-1)-\eta(t-1))-...-\alpha_n(y(t-n)-\eta(t-n))+\beta_0(\overline{u}(t)-\varepsilon(t)))+...+\beta_n(\overline{u}(t-n)-\varepsilon(t-n)), \quad \forall t=n+1,...,N \\ \eta(t)\leq\Delta\eta \\ \eta(t)\geq-\Delta\eta \\ \varepsilon(t)\leq\Delta\varepsilon \\ \varepsilon(t)\geq-\Delta\varepsilon, \quad \forall t=1,...,N}} \theta_i$$

This is a nonconvex polynomial optimization problem and its global optimal solution can be computed by means of convex relaxation approaches. The idea is to replace the nonconvex set with a convex approximation (some uncertainty is introduced) such that:

$$\lim_{\delta \to \infty} PUI^{\delta} = PUI$$

When the *relaxation order* δ tends to ∞, the optimal solution of the convex relaxation converges to the global optimum of the original Polynomial Optimization Problem (POP).

2.3 Identification of MIMO systems

Consider a system defined as follow:

- Linear Time Invariant
- Discrete Time
- Affected by bounded Error In Variable noise
- Multi Input Multi Output

Figure 2.5: MIMO system with p inputs and q outputs

G is the matrix of transfer functions such that:

$$w_i(t) = G_{i1}(q^{-1})u1 + G_{i2}(q^{-1})u2 + ... + G_{ip}(q^{-1})up$$

The identification of a MIMO system is equivalent to the identification of a MISO (Multi Input Single Output) system, so the following formulation is based on a generic MISO system.

2.3.1 Slack Variables Approach

The goal is to identify the parameters of G_1, G_2,...,G_p

$$w(t) = G_1(q^{-1})u1 + G_2(q^{-1})u2 + ... + G_p(q^{-1})up$$

Considering the partial outputs:

$$w(t) = z_1(t) + z_2(t) + ... + z_p(t)$$

where

$$z_1(t) = G_1(q^{-1})u1(t)$$
$$z_2(t) = G_2(q^{-1})u2(t)$$
$$z_p(t) = G_p(q^{-1})up(t)$$

The a-priori informations on the plant and on the noise are:

- $F : w(t) = z_1(t) + z_2(t) + ... + z_p(t), \qquad z_i(t) = G_i(q^{-1})ui(t)$
- noise structure: Error In Variables

The Feasible Parameter Set is defined as:

$$\begin{gathered} D_\theta = \{\theta \in \Re^{\sum_{i=1}^{p} n_i m_i} : w(t) = z_1(t) + z_2(t) + ... + z_p(t), \\ z_i(t) = \frac{\beta_0^i + \beta_1^i q^{-1} + ... + \beta_{mi}^i q^{-mi}}{1 + \alpha_1^i q^{-1} + ... + \alpha_{ni}^i q^{-ni}} u_i(t), \forall i = 1, ..., p \\ w(t) = y(t) - \eta(t), \quad |\eta(t)| \leq \Delta\eta, \\ u_i(t) = \overline{u_i}(t) - \varepsilon_i(t), \quad |\varepsilon(t)| \leq \Delta\varepsilon, \forall t = k, ..., N\} \end{gathered}$$

where k is the largest order of the different transfer functions plus 1. The Extended Feasible Parameter Set is:

$$\begin{gathered} D_{\theta,\eta_i,\varepsilon_i,z_i} = \{\theta \in \Re^{\sum_{i=1}^{p} n_i m_i}, \eta_i \in \Re^N, \varepsilon_i \in \Re^N, z_i \in \Re^N : \\ y(t) - \eta(t) = z_1(t) + z_2(t) + ... + z_p(t), \\ z_i(t) = -\alpha_1^i z_i(t-1) - ... - -\alpha_{ni}^i z_i(t-ni) + \beta_0^i(\overline{u_i}(t) - \varepsilon_i(t)) + ... + \beta_{mi}^i(\overline{u_i}(t-mi) - \varepsilon_i(t-mi)), \\ \eta_i(t) \leq \Delta\eta, \\ \eta_i(t) \geq -\Delta\eta, \\ \varepsilon_i(t) \leq \Delta\varepsilon, \\ \varepsilon_i(t) \geq -\Delta\varepsilon, \\ \forall i = 1, ..., p, \quad \forall t = k, ..., N\} \end{gathered}$$

And the Parameter Uncertainty Intervals are:

$$PUI = [\underline{\theta}_i, \overline{\theta}_i]$$

$$\underline{\theta}_i = \min_{\theta,\eta_i,\varepsilon_i,z_i \in D_{\theta,\eta_i,\varepsilon_i,z_i}} \theta_i$$

$$\overline{\theta}_i = \max_{\theta,\eta_i,\varepsilon_i,z_i \in D_{\theta,\eta_i,\varepsilon_i,z_i}} \theta_i$$

where

$$\underline{\theta}_i = \min_{\substack{s.t. \\ y(t)-\eta(t)=z_1(t)+z_2(t)+...+z_p(t) \\ z_i(t)=-\alpha_1^i z_i(t-1)-...--\alpha_{ni}^i z_i(t-ni)+\beta_0^i(\overline{u_i}(t)-\varepsilon_i(t))+...+\beta_{mi}^i(\overline{u_i}(t-mi)-\varepsilon_i(t-mi)) \\ \eta(t)\leq\Delta\eta \\ \eta(t)\geq-\Delta\eta \\ \varepsilon(t)\leq\Delta\varepsilon \\ \varepsilon(t)\geq-\Delta\varepsilon, \quad \forall i=1,...,p, \quad \forall t=k,...N}} \theta_i$$

and

$$\overline{\theta}_i = \max_{\substack{s.t. \\ y(t)-\eta(t)=z_1(t)+z_2(t)+...+z_p(t) \\ z_i(t)=-\alpha_1^i z_i(t-1)-...--\alpha_{ni}^i z_i(t-ni)+\beta_0^i(\overline{u_i}(t)-\varepsilon_i(t))+...+\beta_{mi}^i(\overline{u_i}(t-mi)-\varepsilon_i(t-mi)) \\ \eta(t)\leq\Delta\eta \\ \eta(t)\geq-\Delta\eta \\ \varepsilon(t)\leq\Delta\varepsilon \\ \varepsilon(t)\geq-\Delta\varepsilon, \quad \forall i=1,...,p, \quad \forall t=k,...N}} \theta_i$$

Chapter 3

Virtual Sensor

3.1 ISWEC model and problem formulation

Since on the ISWEC prototype none sensor is available to measure the Pitch Force, it is possible to collect these data by means of a first-principles based simulator [4].
The simulated system is MISO(Multi Input Single Output)and its output is the Pitch Force while the five inputs, coming from the on board sensors, are:

- x_P Pitch Position [m]
- v_P Pitch Velocity [m/s]
- a_S Surge Acceleration [m/s^2]
- a_H Heave Acceleration [m/s^2]
- F_R Gyroscope Reaction Force [N]

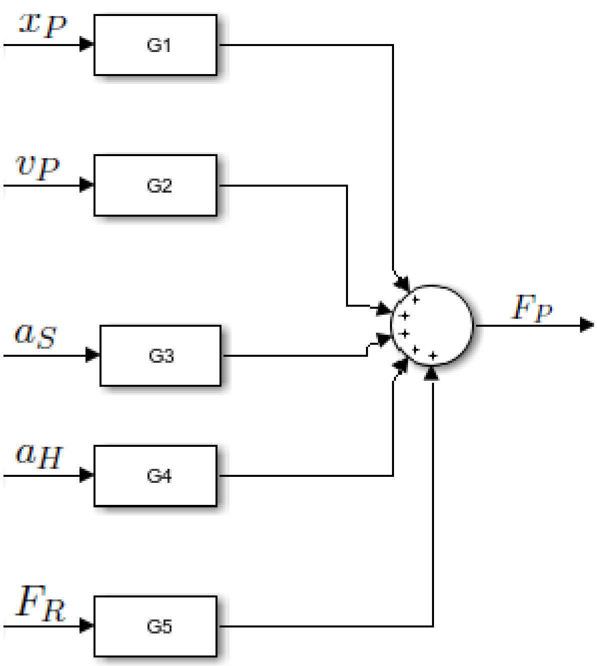

Figure 3.1: 5 inputs, 1 output system

The goal of this chapter is identifying the five transfer functions describing the dynamics between the five inputs and the Pitch Force, through the Set Membership approach.

After an initial attempt with the Least Square method, it is possible to assert that a plausible structure for the five transfer functions is the following:

$$G_i = \frac{\beta_1^i q^{-1} + \beta_2^i q^{-2} + \beta_3^i q^{-3} + \beta_4^i q^{-4} + \beta_5^i q^{-5}}{1 + \alpha_1^i q^{-1} + \alpha_2^i q^{-2} + \alpha_3^i q^{-3} + \alpha_4^i q^{-4} + \alpha_5^i q^{-5}} \tag{3.1}$$

The ISWEC identification problem is an OE (output error) problem, since input data coming from the on board sensors are accurate while the output data are generated by a simulator and consequently they are affected by simulation error.
Being a MISO system, the problem could be solved by the Slack Variables Approach.

3.1.1 Slack Variables Approach for ISWEC

The a priori informations on the plant are:

- Linear Time Invariant
- Discrete Time
- Fifth order

$$F : w(t) = G_1(q^{-1})u1(t) + G_2(q^{-1})u2(t) + G_3(q^{-1})u3(t) + G_4(q^{-1})u4(t) + G_5(q^{-1})u5(t) \tag{3.2}$$

Considering the partial outputs

$$w(t) = z_1(t) + z_2(t) + z_3(t) + z_4(t) + z_5(t) \tag{3.3}$$

and the a priori informations on noise are:

- Output Error structure
- Unknown but bounded

The goal is to identify the parameters α_i and β_i of G_1, G_2, G_3, G_4 and G_5. The set of all the feasible solution is given by the Feasible Parameter Set:

$$\begin{aligned}
&D_\theta = \{\theta \in \Re^5 0 : w(t) = z_1(t) + z_2(t) + z_3(t) + z_4(t) + z_5(t),\\
&z_1(t) = \frac{\beta_1^1 q^{-1} + \beta_2^1 q^{-2} + \beta_3^1 q^{-3} + \beta_4^1 q^{-4} + \beta_5^1 q^{-5}}{1 + \alpha_1^1 q^{-1} + \alpha_2^1 q^{-2} + \alpha_3^1 q^{-3} + \alpha_4^1 q^{-4} + \alpha_5^1 q^{-5}} u1(t),\\
&z_2(t) = \frac{\beta_1^2 q^{-1} + \beta_2^2 q^{-2} + \beta_3^2 q^{-3} + \beta_4^2 q^{-4} + \beta_5^2 q^{-5}}{1 + \alpha_1^2 q^{-1} + \alpha_2^2 q^{-2} + \alpha_3^2 q^{-3} + \alpha_4^2 q^{-4} + \alpha_5^2 q^{-5}} u2(t),\\
&z_3(t) = \frac{\beta_1^3 q^{-1} + \beta_2^3 q^{-2} + \beta_3^3 q^{-3} + \beta_4^3 q^{-4} + \beta_5^3 q^{-5}}{1 + \alpha_1^3 q^{-1} + \alpha_2^3 q^{-2} + \alpha_3^3 q^{-3} + \alpha_4^3 q^{-4} + \alpha_5^3 q^{-5}} u3(t),\\
&z_4(t) = \frac{\beta_1^4 q^{-1} + \beta_2^4 q^{-2} + \beta_3^4 q^{-3} + \beta_4^4 q^{-4} + \beta_5^4 q^{-5}}{1 + \alpha_1^4 q^{-1} + \alpha_2^4 q^{-2} + \alpha_3^4 q^{-3} + \alpha_4^4 q^{-4} + \alpha_5^4 q^{-5}} u4(t),\\
&z_5(t) = \frac{\beta_1^5 q^{-1} + \beta_2^5 q^{-2} + \beta_3^5 q^{-3} + \beta_4^5 q^{-4} + \beta_5^5 q^{-5}}{1 + \alpha_1^5 q^{-1} + \alpha_2^5 q^{-2} + \alpha_3^5 q^{-3} + \alpha_4^5 q^{-4} + \alpha_5^5 q^{-5}} u5(t),\\
&w(t) = y(t) - \eta(t), \quad |\eta(t)| \le \Delta\eta, \quad \forall t = 6, ..., N\}
\end{aligned}$$

The Extended Feasible Parameter Set is:

$$
\begin{aligned}
&D_{\theta,\eta,z_i} = \{\theta \in \Re^5 0, \eta \in \Re^N, z_1 \in \Re^N, z_2 \in \Re^N, z_3 \in \Re^N, z_4 \in \Re^N, z_5 \in \Re^N : \\
&y(t) - \eta(t) = z_1(t) + z_2(t) + z_3(t) + z_4(t) + z_5(t), \\
&z_1(t) = -\alpha_1^1 z_1(t-1) - \alpha_2^1 z_1(t-2) - \alpha_3^1 z_1(t-3) - \alpha_4^1 z_1(t-4) - \alpha_5^1 z_1(t-5) + \\
&+ \beta_1^1 u1(t-1) + \beta_2^1 u1(t-2) + \beta_3^1 u1(t-3) + \beta_4^1 u1(t-4) + \beta_5^1 u1(t-5), \\
\\
&z_2(t) = -\alpha_1^2 z_2(t-1) - \alpha_2^2 z_2(t-2) - \alpha_3^2 z_2(t-3) - \alpha_4^2 z_2(t-4) - \alpha_5^2 z_2(t-5) + \\
&+ \beta_1^2 u2(t-1) + \beta_2^2 u2(t-2) + \beta_3^2 u2(t-3) + \beta_4^2 u2(t-4) + \beta_5^2 u2(t-5), \\
\\
&z_3(t) = -\alpha_1^3 z_3(t-1) - \alpha_2^3 z_3(t-2) - \alpha_3^3 z_3(t-3) - \alpha_4^3 z_3(t-4) - \alpha_5^3 z_3(t-5) + \\
&+ \beta_1^3 u3(t-1) + \beta_2^3 u3(t-2) + \beta_3^3 u3(t-3) + \beta_4^3 u3(t-4) + \beta_5^3 u3(t-5), \\
\\
&z_4(t) = -\alpha_1^4 z_4(t-1) - \alpha_2^4 z_4(t-2) - \alpha_3^4 z_4(t-3) - \alpha_4^4 z_4(t-4) - \alpha_5^4 z_4 3(t-5) + \\
&+ \beta_1^4 u4(t-1) + \beta_2^4 u4(t-2) + \beta_3^4 u4(t-3) + \beta_4^4 u4(t-4) + \beta_5^4 u4(t-5), \\
\\
&z_5(t) = -\alpha_1^5 z_5(t-1) - \alpha_2^5 z_5(t-2) - \alpha_3^5 z_5(t-3) - \alpha_4^5 z_5(t-4) - \alpha_5^5 z_5(t-5) + \\
&+ \beta_1^5 u5(t-1) + \beta_2^5 u5(t-2) + \beta_3^5 u5(t-3) + \beta_4^5 u5(t-4) + \beta_5^5 u5(t-5), \\
&|\eta(t)| \leq \Delta\eta, \quad \forall t = 6, ..., N\}
\end{aligned}
$$

And the Parameter Uncertainty Intervals are:

$$PUI = [\underline{\theta}_i, \overline{\theta}_i]$$

$$\underline{\theta}_i = \min_{\theta,\eta_i,z_i \in D_{\theta,\eta_i,z_i}} \theta_i$$

$$\overline{\theta}_i = \max_{\theta,\eta_i,z_i \in D_{\theta,\eta_i,z_i}} \theta_i$$

where

$$\underline{\theta}_i = \min_{\substack{s.t. \\ y(t)-\eta(t)=z_1(t)+z_2(t)+z_3(t)+z_4(t)+z_5(t) \\ z_i(t)=-\alpha_1^i z_i(t-1)-\alpha_2^i z_i(t-2)-\alpha_3^i z_i(t-3)-\alpha_4^i z_i(t-4)-\alpha_i^5 z_i(t-5)+ \\ +\beta_1^i ui(t-1)+\beta_2^i ui(t-2)+\beta_3^i ui(t-3)+\beta_4^i ui(t-4)+\beta_5^i ui(t-5) \\ \eta(t)\leq\Delta\eta \\ \eta(t)\geq-\Delta\eta \\ \forall i=1,...,5, \quad \forall t=6,...N}} \theta_i$$

and

$$\overline{\theta}_i = \max_{\substack{s.t. \\ y(t)-\eta(t)=z_1(t)+z_2(t)+z_3(t)+z_4(t)+z_5(t) \\ z_i(t)=-\alpha_1^i z_i(t-1)-\alpha_2^i z_i(t-2)-\alpha_3^i z_i(t-3)-\alpha_4^i z_i(t-4)-\alpha_i^5 z_i(t-5)+ \\ +\beta_1^i ui(t-1)+\beta_2^i ui(t-2)+\beta_3^i ui(t-3)+\beta_4^i ui(t-4)+\beta_5^i ui(t-5) \\ \eta(t)\leq\Delta\eta \\ \eta(t)\geq-\Delta\eta \\ \forall i=1,...,5, \quad \forall t=6,...N}} \theta_i$$

The identification was performed considering:

- $\Delta\eta$ infinite
- different values of N (number of samples), N=300,100,70,20
- relaxation order 1 and 2

The obtained results were not able to describe the dynamics of the system, since the problem, formulated as above, is too computationally expensive. An alternative solution is proposed below.

3.2 Incremental Approach

The Incremental Approach consists in identifying five SISO systems ($\overline{G}_1$,$\overline{G}_2$,$\overline{G}_3$,$\overline{G}_4$,$\overline{G}_5$) such that for each system the input comes from the on board sensors while, only for the first system, the output is the simulated Pitch Force. Identifying the second system, the output is the residual between the Pitch Force and the output generated by $\overline{G}_1$, the third output is the residual between the first residual and the output generated by $\overline{G}_2$ etc.
The identification is built on 5 steps:

1. $\overline{G}_1$ identification: input u1 and output F_P
2. $\overline{G}_2$ identification: input u2 and output $F_P - u1\overline{G}_1$
3. $\overline{G}_3$ identification: input u3 and output $F_P - u1\overline{G}_1 - u2\overline{G}_2$
4. $\overline{G}_4$ identification: input u4 and output $F_P - u1\overline{G}_1 - u2\overline{G}_2 - u3\overline{G}_3$
5. $\overline{G}_5$ identification: input u5 and output $F_P - u1\overline{G}_1 - u2\overline{G}_2 - u3\overline{G}_3 - u4\overline{G}_4$

and the total output is given by the sum of the five simulated output:

$$y_t = z1 + z2 + z3 + z4 + z5$$

Some initial informations are needed:

- $\overline{G}_i$ structure
- bound on the error

3.2.1 $\overline{G}_i$ structure

The idea is to find the simplest possible model in order to reduce the complexity of the total system. Starting from the Least Square Method it is possible to have an idea of the best structure, evaluating the results coming from different order systems and varying the number of inputs. In the following table are reported the values of the Goodness of Fit index linked to sundry models, identified by means of LS method considering the first 3000 samples of Data Set 84.

$$GoF = 1 - \sqrt{\frac{\sum_{i=1}^{N}(F_P(t) - F_{Pe}(t))^2}{\sum_{i=1}^{N}(F_P(t))^2}} \tag{3.5}$$

As shown in 3.1 the best solution is given by the fifth order, five inputs model but looking for a simpler one, a good alternative is a two inputs model. In order to understand which could be a better order for the system, it is necessary to evaluate the results, in terms of accuracy, coming from the validation of the 2-input (u1 and u3) model on the other data sets.

Table 3.1: GoF index for LS identification

	Order				
Input	**1**	**2**	**3**	**4**	**5**
u1,u2,u3,u4,u5	54%	91%	30%	-	98%
u1,u2,u3,u4	82%	88%	92%	95%	30%
u1,u2,u3	81%	92%	91%	94%	6%
u1,u2	52%	73%	60%	6%	61%
u1,u3	83%	91%	93%	94%	96%

Table 3.2: GoF index in validation

	Order				
Data Set	**1**	**2**	**3**	**4**	**5**
86	88%	89%	91%	88%	95%
125	89%	88%	90%	80%	94%
48	86%	88%	92%	90%	95%
46	86%	91%	94%	94%	97%
44	27%	64%	71%	67%	79%
08	70%	82%	91%	90%	96%
06	63%	82%	90%	89%	94%

Looking at 3.1 and 3.3 it is evident that the best models are:

1. 2-inputs (u1 and u3), third order
2. 2-inputs (u1 and u3), fifth order

but a simpler solution could be represented by the 2-inputs, second order model. This represents the least complex model possible with a good accuracy.

3.2.2 Bound on the error

In this case η is not the simulation error but it is the error that is made in trying to explain the output in function of a single input, in place of all five. η is defined as

$$y - w = \eta, \qquad |\eta| \leq \Delta\eta$$

where

- y is the Pitch Force for the first step and the residual for the others
- w is the output generated by the identified system given a single input

$\Delta\eta$ is estimated solving the following minimization problem.

$$\begin{gathered}\Delta\eta = \min_{s.t.} t \\ y(t)-\eta(t)=-\alpha_1^i(y(t-1)-\eta(t-1))-\ldots-\alpha_n^i(y(t-n)-\eta(t-n))+ \\ +\beta_1^i ui(t-1)+\ldots+\beta_n^i ui(t-n) \\ \eta(t)\leq t \\ -\eta(t)\leq -t \\ \forall i=1,\ldots,k, \quad \forall t=n+1,\ldots N\end{gathered}$$

- N is the number of samples
- n is the order of $\overline{G}_i$
- k is the number of inputs

3.3 2-Inputs, Second Order Model

The goal is to identify the 8 parameters of the 2-input Model through the Incremental Approach, the problem is solved by splitting the SISO identification in 2 further steps:

1. Error Minimization
2. Parameters Identification

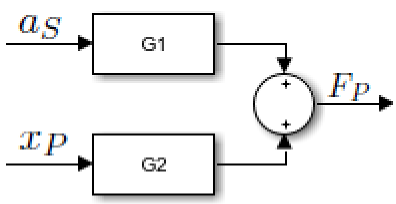

Figure 3.2: 2-Input Model

3.3.1 Error Minimization

The Error Minimization Problem is solved as explained in 3.2.2 and $\Delta\eta$ is estimated solving the following minimization problem.

$$\begin{gathered}\Delta\eta = \min \theta_i \\ s.t. \\ y(t)-\eta(t)=-\alpha_1^i(y(t-1)-\eta(t-1))+ \\ -\alpha_n^i(y(t-2)-\eta(t-2))+\beta_1^i ui(t-1)+\beta_n^i ui(t-2) \\ \eta(t)\le t \\ -\eta(t)\le -t \\ \forall i=1,2, \quad \forall t=3,...N\end{gathered}$$

Knowing $\Delta\eta$ is possible to proceed with the System Identification.

3.3.2 Parameters Identification

At this point it is possible to identify the parameters α_i and β_i of G_1 and G_2. The set of all the feasible solution is given by the Feasible Parameter Set:

$$\begin{aligned}&D_\theta = \{\theta \in \Re^4 : w_i(t) = \frac{\beta_1^i q^{-1} + \beta_2^i q^{-2}}{1+\alpha_1^i q^{-1} + \alpha_2^i q^{-2}} ui(t), \quad \forall i = 1,2 \\ &w(t) = y(t) - \eta(t), \\ &|\eta(t)| \le \Delta\eta, \quad \forall t = 3, ..., N\}\end{aligned}$$

The Extended Feasible Parameter Set is:

$$\begin{aligned}&D_{\theta,\eta} = \{\theta \in \Re^4, \eta \in \Re^N : w(t) - \eta(t) = -\alpha_1^i(y(t-1) - \eta(t-1))+ \\ &-\alpha_n^i(y(t-2) - \eta(t-2)) + \beta_1^i ui(t-1) + \beta_n^i ui(t-2)), \quad \forall i = 1,2 \\ &|\eta(t)| \le \Delta\eta, \quad \forall t = 3, ..., N\}\end{aligned}$$

And the Parameter Uncertainty Intervals are:

$$PUI = [\underline{\theta}_i, \overline{\theta}_i]$$

$$\underline{\theta}_i = \min_{\theta,\eta_i \in D_{\theta,\eta_i}} \theta_i$$

$$\overline{\theta}_i = \max_{\theta,\eta_i \in D_{\theta,\eta_i}} \theta_i$$

where

$$\underline{\theta}_i = \min_{\substack{s.t.\\ w(t)-\eta(t)=-\alpha_1^i(y(t-1)-\eta(t-1))+\\ -\alpha_n^i(y(t-2)-\eta(t-2))+\beta_1^i ui(t-1)+\beta_n^i ui(t-2)), \quad \forall i=1,2\\ |\eta(t)|\leq\Delta\eta, \quad \forall t=3,\ldots,N}} \theta_i$$

and

$$\overline{\theta}_i = \max_{\substack{s.t.\\ w(t)-\eta(t)=-\alpha_1^i(y(t-1)-\eta(t-1))+\\ -\alpha_n^i(y(t-2)-\eta(t-2))+\beta_1^i ui(t-1)+\beta_n^i ui(t-2)), \quad \forall i=1,2\\ |\eta(t)|\leq\Delta\eta, \quad \forall t=3,\ldots,N}} \theta_i$$

So that the Incremental Approach works, it is important to identify as first system the one corresponding to the input which has the greatest impact on the overall output.
Considering the model identified with the Least Square and simulating each system with the corresponding input it is possible to compare the output with the Pitch Force.

From 3.3 and it is evident that the Surge Acceleration has a greater impact on the Pitch Force, it leads to a GoF of 60.7% while the Pitch Position to -19%. According to these considerations

- $u1 = Surge \quad Acceleration$
- $u2 = Pitch \quad Position$

From the computational point of view, the identification of α_i and β_i is not expensive since it deals with a SISO second order system and moreover the problem can be reasonably simplified to an Error Minimization Problem.
This last statement is justified by the fact that in this specific case the error η is not the simulation error but the error that is made in trying to explain the output in function of a single input, consequently there is no need to calculate the PUIs since the optimal solution is represented by those parameters that minimize the error η. This means that the identification of the 2-inputs, second order system can be performed by solving the problem formulated in 3.3.1.

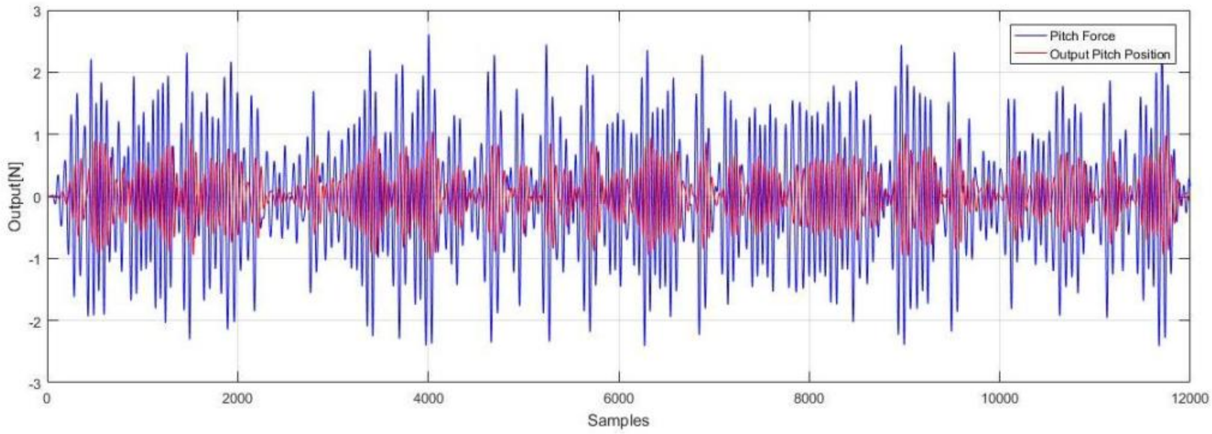

Figure 3.3: a) Comparison between the Pitch Force and the output corresponding to the Pitch Position

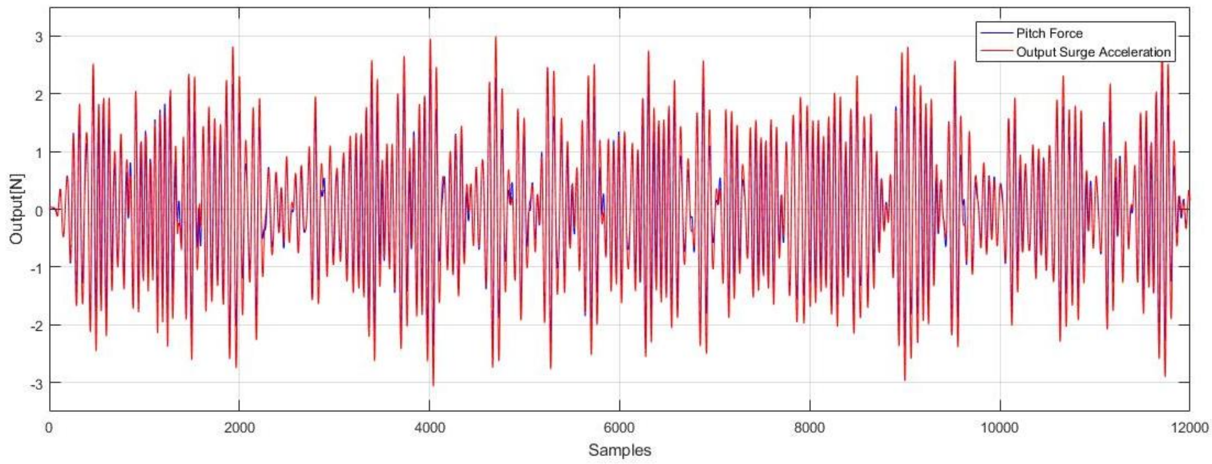

Figure 3.4: b) Comparison between the Pitch Force and the output corresponding to the Surge Acceleration

3.4 Results and Considerations

Assured that the identification problem can be solved by simply minimizing the error, the whole problem is reduced from 4 to just 2 steps:

1. Minimization of the Error for the first system
2. Minimization of the Error for the second system

3.4.1 First Error Minimization

The error minimization problem for the system with input $u1 = SurgeAcceleration$ has been solved on 121 samples of Data Set 84 and validated on the entire data set and on the others.
The identification leads to a GoF of 91.8% that becomes 82.64% in validation on the entire data set, as shown in 3.5 and 3.6.

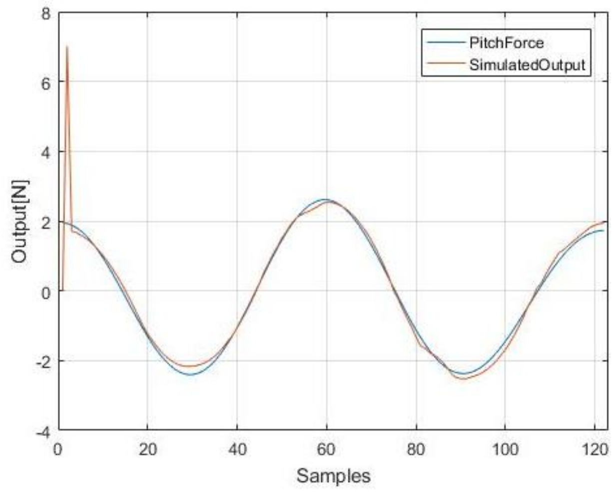

Figure 3.5: Comparison between the Pitch Force and the generated output on the identification data set

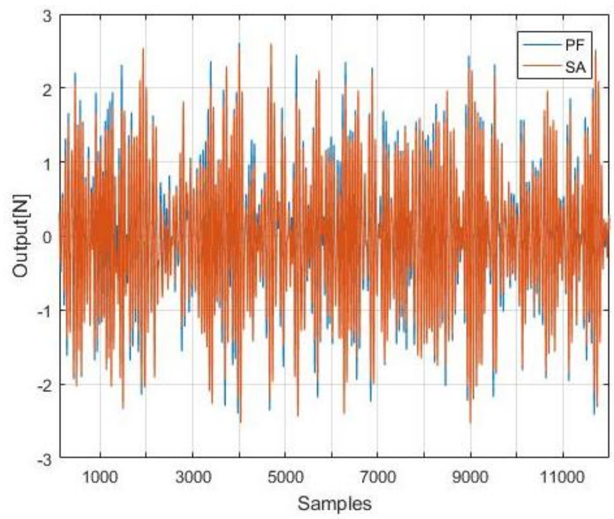

Figure 3.6: Comparison between the Pitch Force and the generated output on the validation data set

The values of the Goodness of Fit index for the validation on the other data set are reported in the following table:

Table 3.3: GoF values in validation

Data Set	**GoF**
06	68.9%
08	75%
44	39.6%
46	86.3%
48	83.8%
86	86%
125	86.9%

Looking at 3.3 and the following figures it is clear that for Data Set 06,08 and 44 the identified model is not able to represent accurately the real system while for the other Data Sets the behaviour is quiet good.

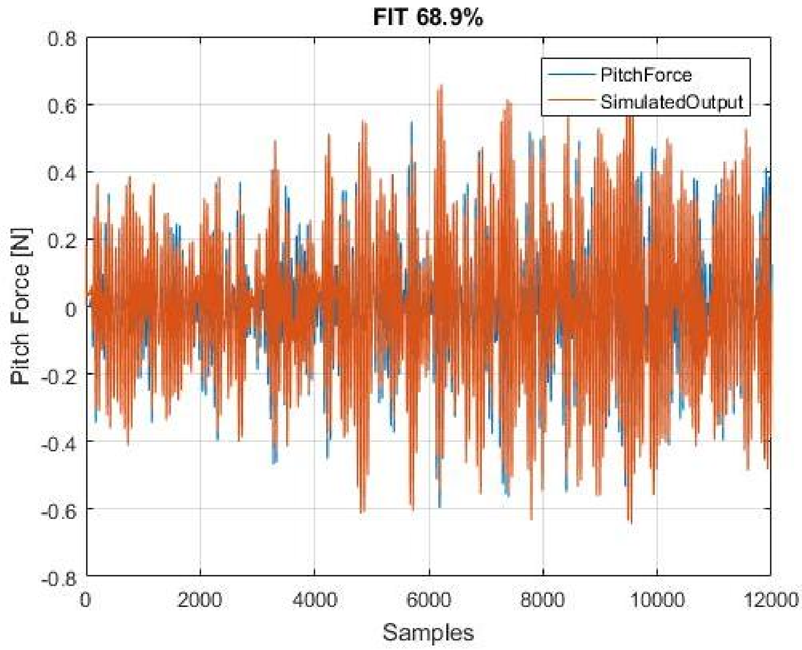

Figure 3.7: Validation on Data Set 06

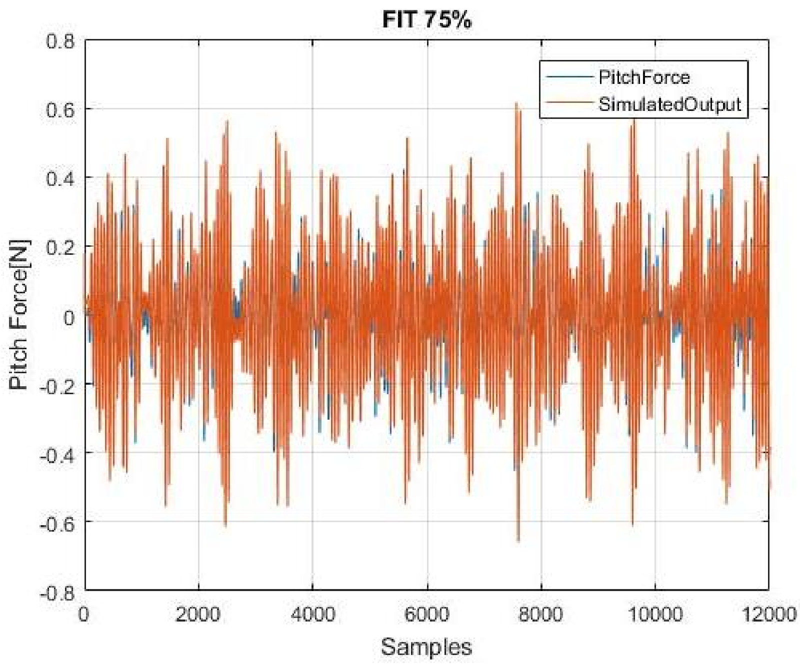

Figure 3.8: Validation on Data Set 08

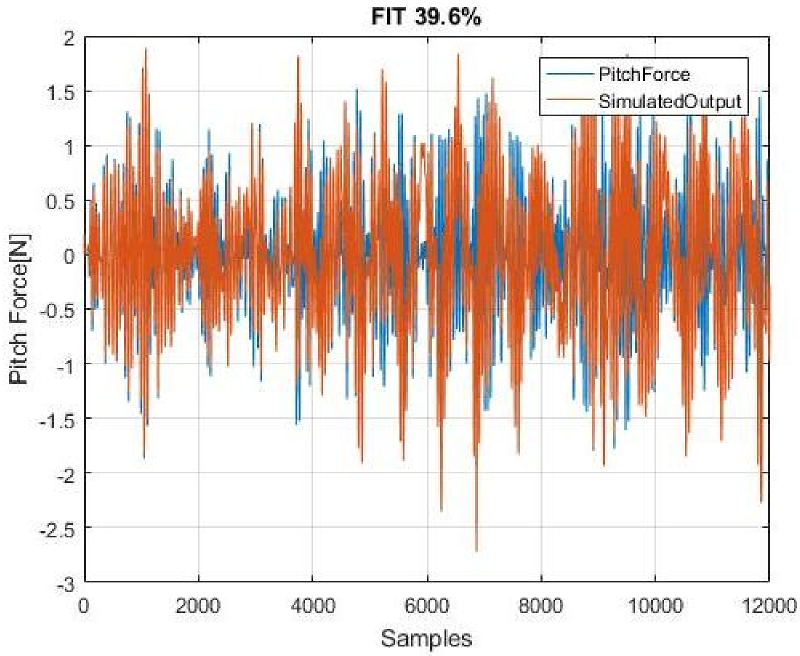

Figure 3.9: Validation on Data Set 44

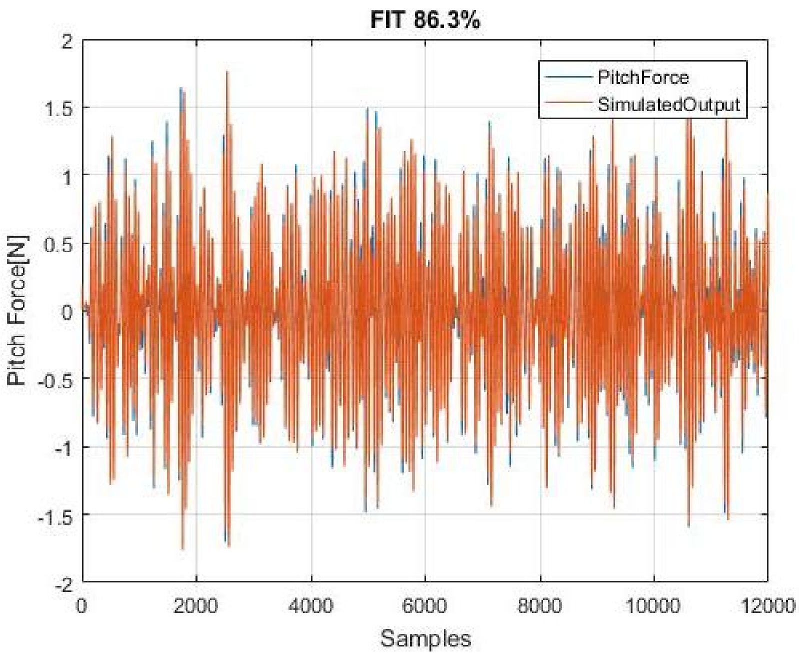

Figure 3.10: Validation on Data Set 46

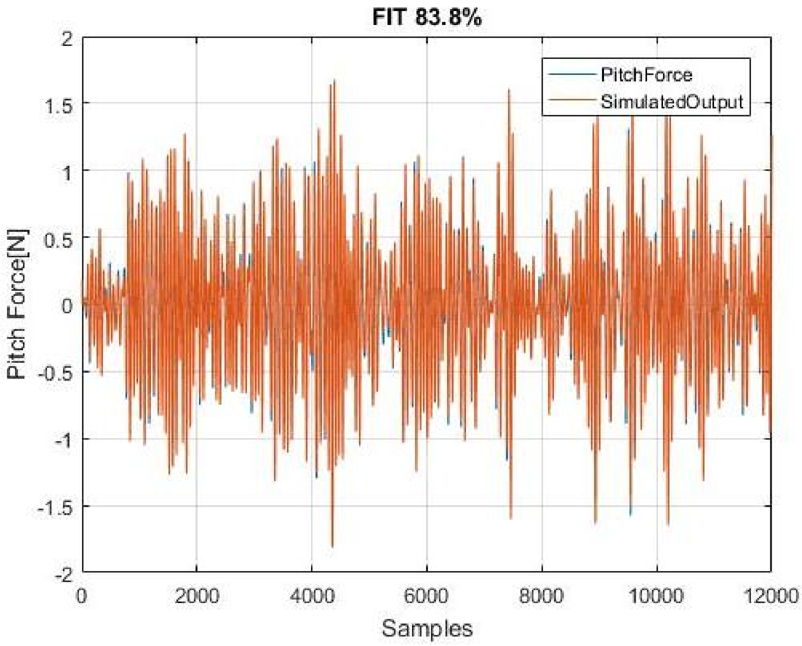

Figure 3.11: Validation on Data Set 48

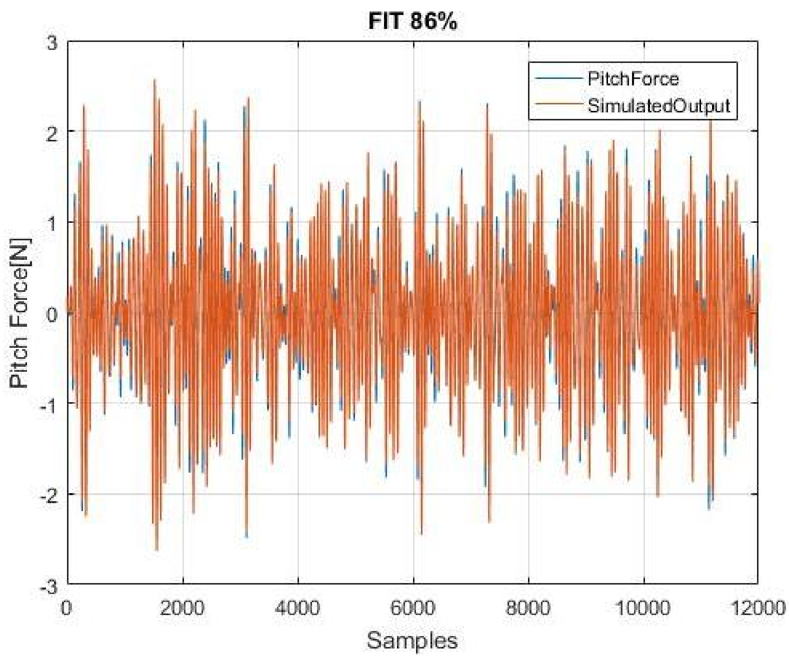

Figure 3.12: Validation on Data Set 86

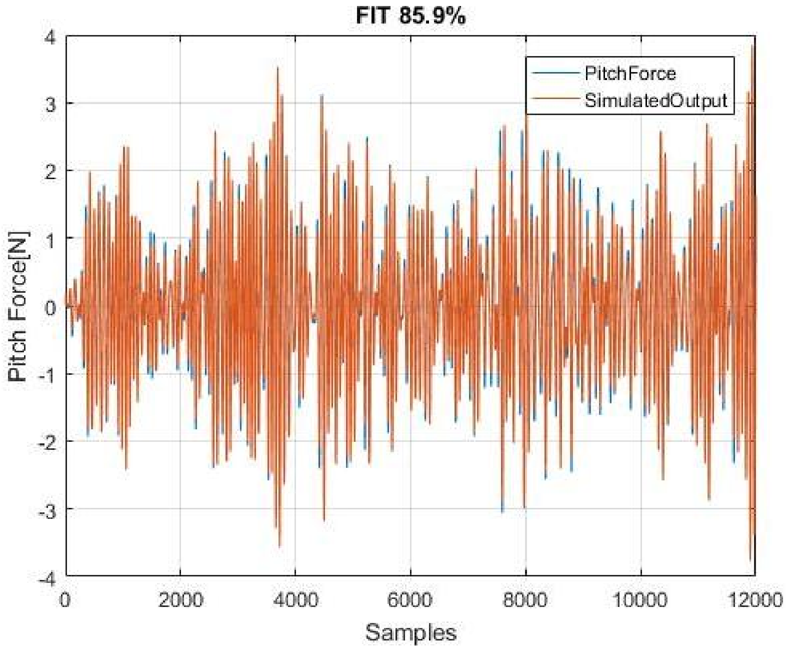

Figure 3.13: Validation on Data Set 125

3.4.2 Second Error Minimization

While for the first step the output is represented by the Pitch Force, in this case the output is the residual $F_P - u1\overline{G}_1$, where:

- F_P is the Pitch Force
- u1 is the Surge Acceleration
- $\overline{G}_1$ is the first identified system
- $u1\overline{G}_1$ is the first simulated output

Since the residual is closed to zero, solving this minimization problem leads to an identified system which input is the Pitch Position but its output does not track the residual, as shown in 3.14.
The second identified system has no effect on the overall system output, in fact adding together the outputs of the two identified systems the value of the GoF index does not vary, it is still 82.64% and the behaviour of the simulated output (3.15) is the same as the case with just the first input (3.6).
In conclusion, a further simplification can be introduced:
The Surge Acceleration is sufficient to describe the behavior of the system. Thanks to the Incremental Approach it was possible to prove that the 5 inputs system can be satisfactorily described by a SISO model which input is the Surge Acceleration. This result must be verified during the prediction phase.

It is worth quickly demonstrating that the other inputs do not allow to obtain better results. Solving the Minimization Error problem varying the input, the obtained results in terms of GoF are reported in Table 3.4. It is evident that the best fitting is given by the identified system from the Surge Acceleration input. Furthermore, it may be useful to note that the Reaction Force has a negligible effect on the overall system.

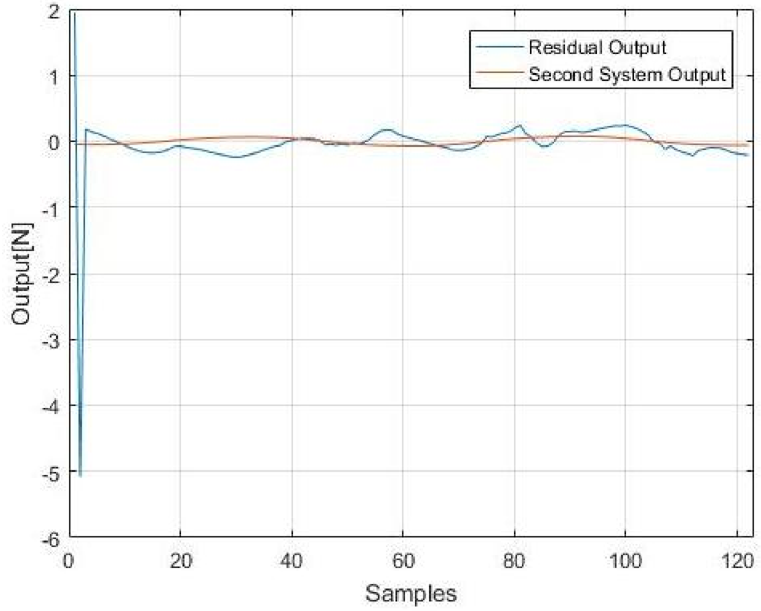

Figure 3.14: Comparison between the Residual Output and the Simulated Output

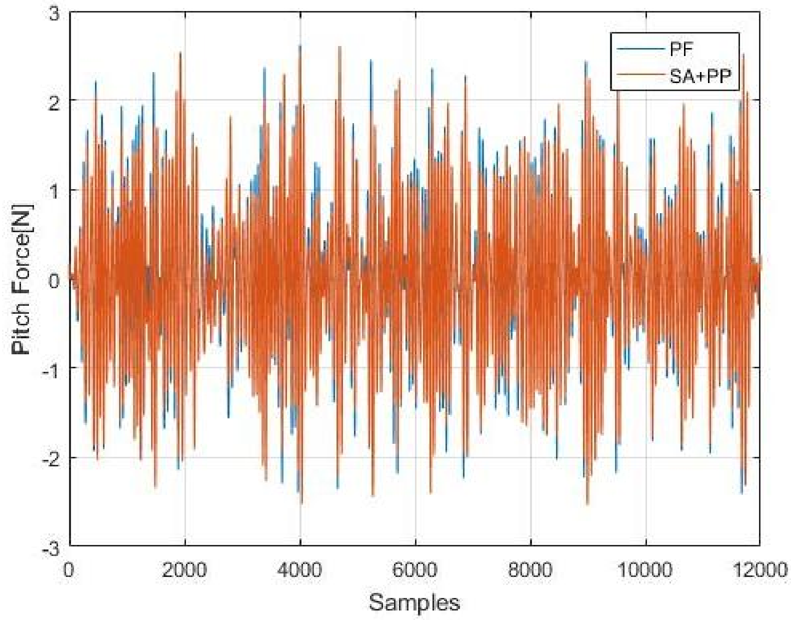

Figure 3.15: Comparison between the Pitch Force and the simulated total output

Table 3.4: FIT values First Step

Input	**GoF**
Surge Acceleration	82.64%
Heave Acceleration	53.65%
Pitch Velocity	50.67%
Pitch Position	62.22%
Reaction Force	-30.89%

Chapter 4

Predictor

As explained above, the goal of this thesis is to predict the Pitch Force in view of a Predictive Control to optimize the ISWEC performance. After the identification phase, it is possible to predict the Pitch Force using an Auto Regressive (AR) Model

$$\widehat{y}(t+\Delta|t) = \alpha_1 y_s(t) + \alpha_i y_s(t-1) + ... + \alpha_n y_s(t-n) \tag{4.1}$$

according to the standard Least Square approach,minimizing the L_2-norm of the error:

$$\alpha = arg\min_{\alpha} \|e\|_2 = arg\min_{\alpha} \|F_P(t) - \alpha^T \begin{bmatrix} F_P(t-1) \\ . \\ . \\ . \\ F_P(t-n) \end{bmatrix} \|_2 \tag{4.2}$$

where

$$\alpha = \begin{bmatrix} \alpha_0 \\ \alpha_1 \\ . \\ . \\ . \\ \alpha_n \end{bmatrix}$$

$n =$ order of the AR model

4.1 Results

The values of $F_P(t-1), ..., F_P(t-n)$ come from the Virtual Sensor and they are used to identify an Auto Regressive Predictor with different order n and a prediction horizon of 10s. In this section are shown the results coming from the prediction algorithm for $n = 200$ and $n = 10$. The algorithm has been tested on different data sets, data are sampled with a sampling time of 0.1s.

4.1.1 Order n=200

The results obtained for a Predictor of order 200 are reported below, it has been identified using data set 84 and validated on the other data sets.

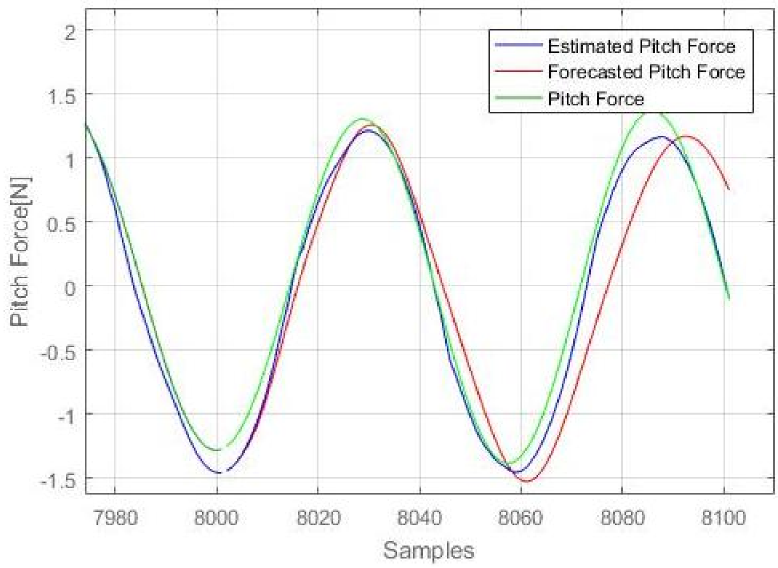

Figure 4.1: Prediction on Data Set 84

In figure 4.1 it is shown the comparison between the Pitch Force simulated by the first-principles based simulator, which inputs belong to Data Set 84, the estimated Pitch Force by the Virtual Sensor and the forecasted Pitch Force. Along the prediction horizon the value of the GoF index between the forcasted output and the estimated one is 66.98%, while between the forecasted and the simulated is 57.56%. The prediction is quiet good for the first 6s with a fitting of 82.9% with the estimated Pitch Force and 78.8% with the simulated.

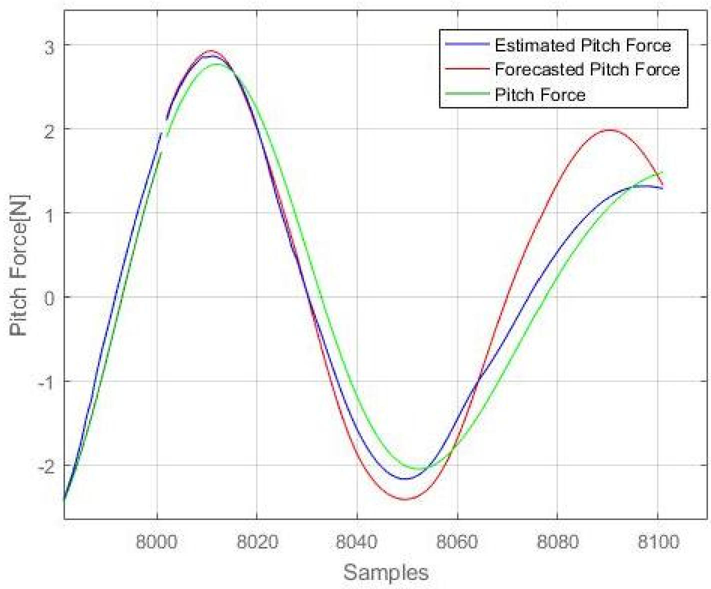

Figure 4.2: Prediction on Data Set 125

In figure 4.2 it is shown the behaviour of the predicted Pitch Force when the data generated by the virtual sensor belong to Data Set 125. Along the prediction horizon the value of the GoF index between the forcasted output and the estimated one is 74.2%, while between the forecasted and the simulated is 61.9%. The prediction is quiet good for the first 4s with a fitting of 93% with the estimated Pitch Force and 78.5% with the simulated while along 6s the fitting is 90.6% with the estimated Pitch Force and 78.8% with the simulated.

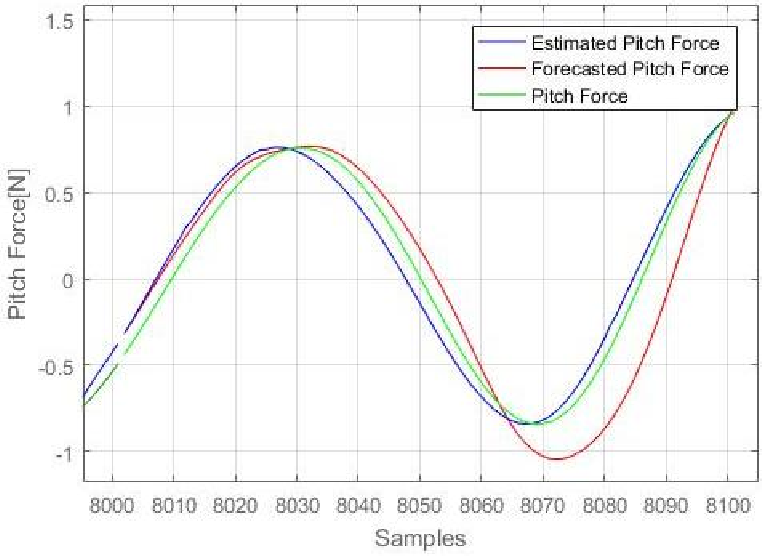

Figure 4.3: Prediction on Data Set 86

In figure 4.3 it is shown the behaviour of the predicted Pitch Force when the data generated by the virtual sensor belong to Data Set 86. Along the prediction horizon the value of the GoF index between the forcasted output and the estimated one is 51.3%, while between the forecasted and the simulated is 62.3%. The prediction is quiet good for the first 4s with a fitting of 93% with the estimated Pitch Force and 78.5% with the simulated while along 4s the fitting is 83.7% with the estimated Pitch Force and 84.3% with the simulated and along 3s the fitting is respectively 93.9% and 80.9%.

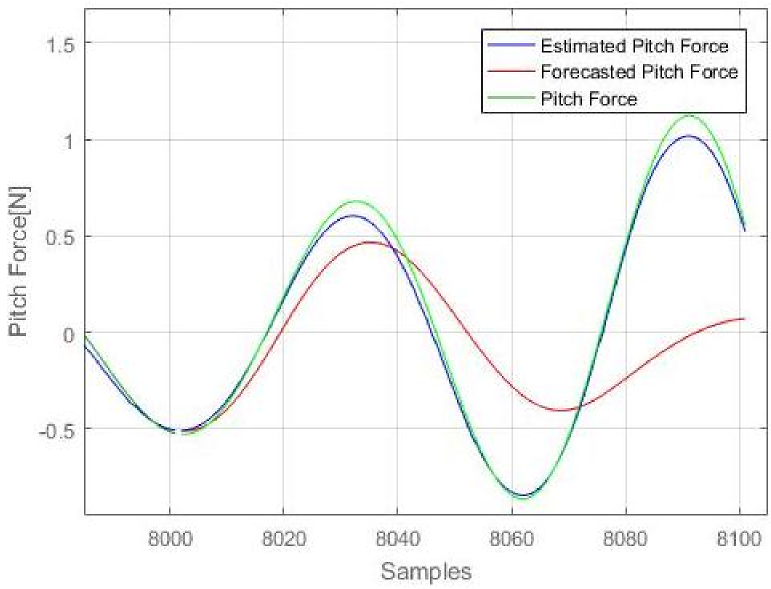

Figure 4.4: Prediction on Data Set 46

In figure 4.4 it is shown the behaviour of the predicted Pitch Force when the data generated by the virtual sensor belong to Data Set 46. Along the prediction horizon the value of the GoF index between the forcasted output and the estimated one is 16.23%, while between the forecasted and the simulated is 16.26%. The prediction is better for the first 1.5s with a fitting of 85.8% with the estimated Pitch Force and 87.9% with the simulated while along 2s the fitting is 75.6% with the estimated Pitch Force and 75.98% with the simulated.

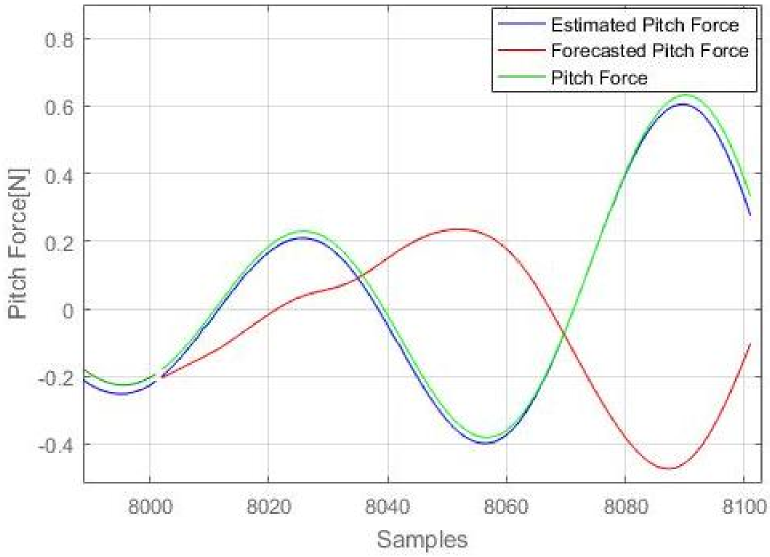

Figure 4.5: Prediction on Data Set 48

In figure 4.5 it is shown the behaviour of the predicted Pitch Force when the data generated by the virtual sensor belong to Data Set 48. Along the prediction horizon the value of the GoF index between the forcasted output and the estimated one is -67.5%, while between the forecasted and the simulated is -65.5%. The prediction is quiet good only for the first 0.5s, with a fitting of 84% with the estimated Pitch Force and 72.5% with the simulated.

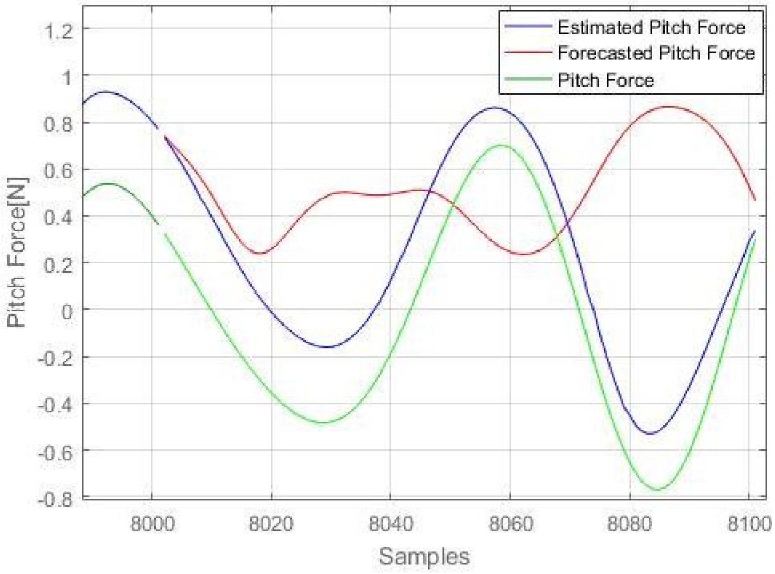

Figure 4.6: Prediction on Data Set 44

In figure 4.6 it is shown the behaviour of the predicted Pitch Force when the data generated by the virtual sensor belong to Data Set 44. Along the prediction horizon the value of the GoF index between the forcasted output and the estimated one is -67.5%, while between the forecasted and the simulated is -65.5%. In this case the predictor is not able to provide a good estimate of the Pitch Force future value, neither for a horizon of few milliseconds.

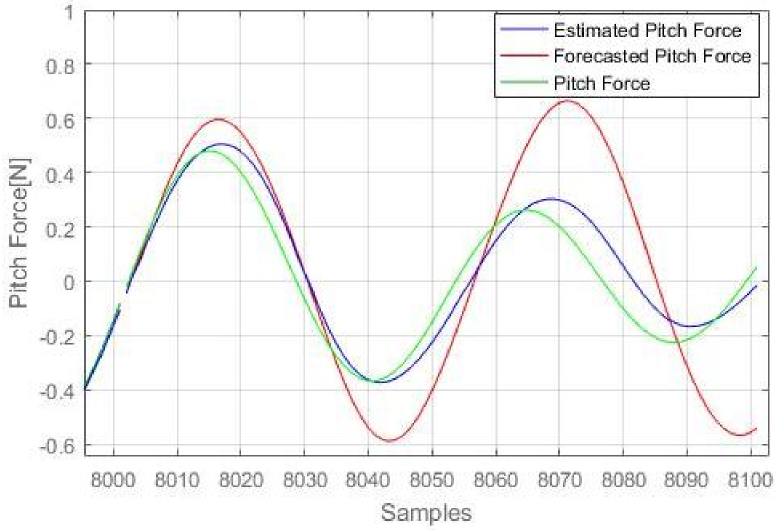

Figure 4.7: Prediction on Data Set 06

In figure 4.7 it is shown the behaviour of the predicted Pitch Force when the data generated by the virtual sensor belong to Data Set 06. Along the prediction horizon the value of the GoF index between the forcasted output and the estimated one is 15.9%, while between the forecasted and the simulated is -11.6%. The prediction improves for the first 2s, with a fitting of 82.97% with the estimated Pitch Force and 76.3% with the simulated.

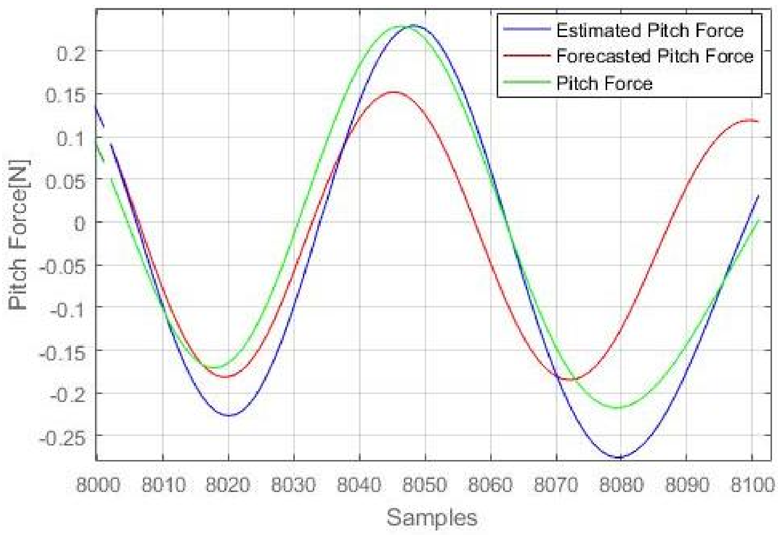

Figure 4.8: Prediction on Data Set 08

In figure 4.8 it is shown the behaviour of the predicted Pitch Force when the data generated by the virtual sensor belong to Data Set 08. Along the prediction horizon the value of the GoF index between the forcasted output and the estimated one is 38.99%, while between the forecasted and the simulated is 37.34%. The prediction improves for the first 2s, with a fitting of 80.9% with the estimated Pitch Force and 79.7% with the simulated.

4.1.2 Order n=10

Let's now consider a predictor of order 10, it has been identified using data set 84 and validated on the other data set.

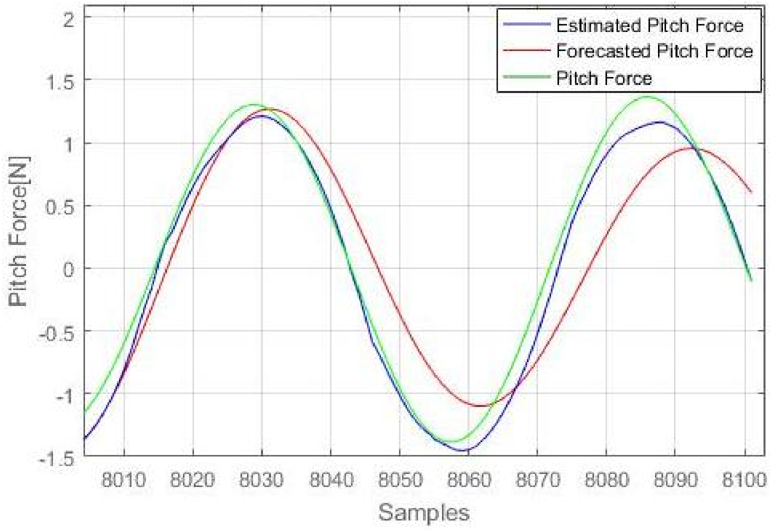

Figure 4.9: Prediction on Data Set 84

In figure 4.9 it is shown the comparison between the Pitch Force simulated by the first-principles based simulator, which inputs belong to Data Set 84, the estimated Pitch Force by the Virtual Sensor and the forecasted Pitch Force. Along the prediction horizon the value of the GoF index between the forcasted output and the estimated one is 60.77%, while between the forecasted and the simulated is 54.4%. The prediction improves in the first 3s with a fitting of 89% with the estimated Pitch Force and 77.7% with the simulated.

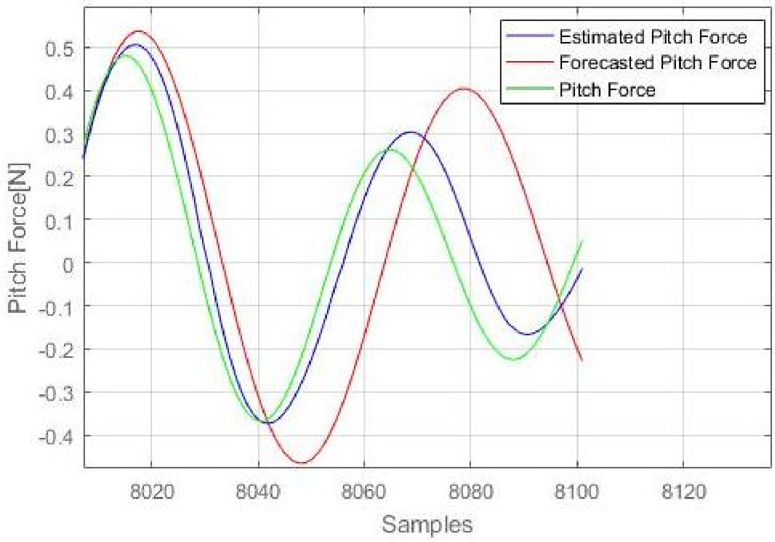

Figure 4.10: Prediction on Data Set 06

In figure 4.10 it is shown the comparison between the Pitch Force simulated by the first-principles based simulator, which inputs belong to Data Set 06, the estimated Pitch Force by the Virtual Sensor and the forecasted Pitch Force. Along the prediction horizon the value of the GoF index between the forcasted output and the estimated one is 22.9%, while between the forecasted and the simulated is -8.99%. The prediction improves in the first 2s with a fitting of 94% with the estimated Pitch Force and 84.6% with the simulated.

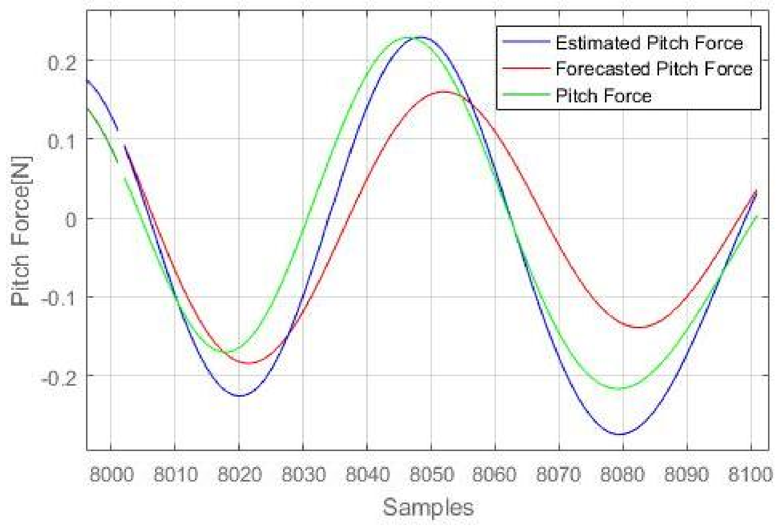

Figure 4.11: Prediction on Data Set 08

In figure 4.11 it is shown the comparison between the Pitch Force simulated by the first-principles based simulator, which inputs belong to Data Set 08, the estimated Pitch Force by the Virtual Sensor and the forecasted Pitch Force. Along the prediction horizon the value of the GoF index between the forcasted output and the estimated one is 52.52%, while between the forecasted and the simulated is 46.85%. The prediction improves in the first 2s with a fitting of 77% with the estimated Pitch Force and 75.5% with the simulated.

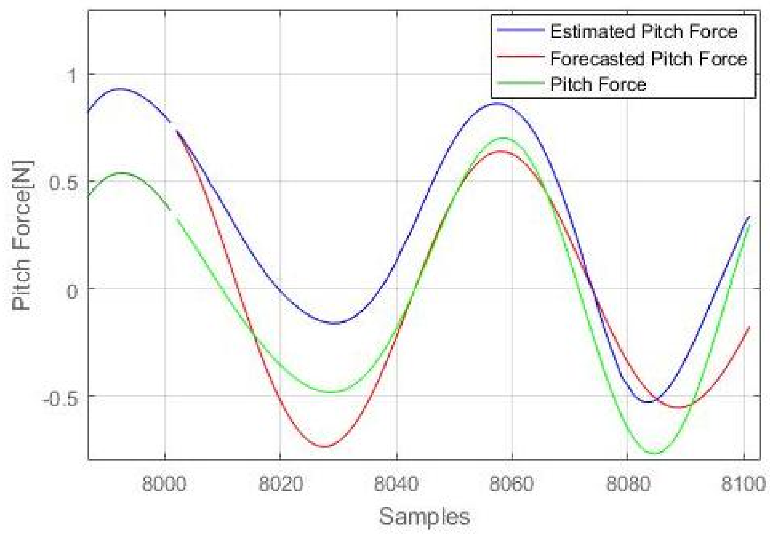

Figure 4.12: Prediction on Data Set 44

In figure 4.12 it is shown the comparison between the Pitch Force simulated by the first-principles based simulator, which inputs belong to Data Set 44, the estimated Pitch Force by the Virtual Sensor and the forecasted Pitch Force. Along the prediction horizon the value of the GoF index between the forcasted output and the estimated one is 27%, while between the forecasted and the simulated is 53.5%.In this case it is particular that the prediction has a good behaviour after 4s up to 7s, the fitting is 63% with the estimated Pitch Force and 90% with the simulated.

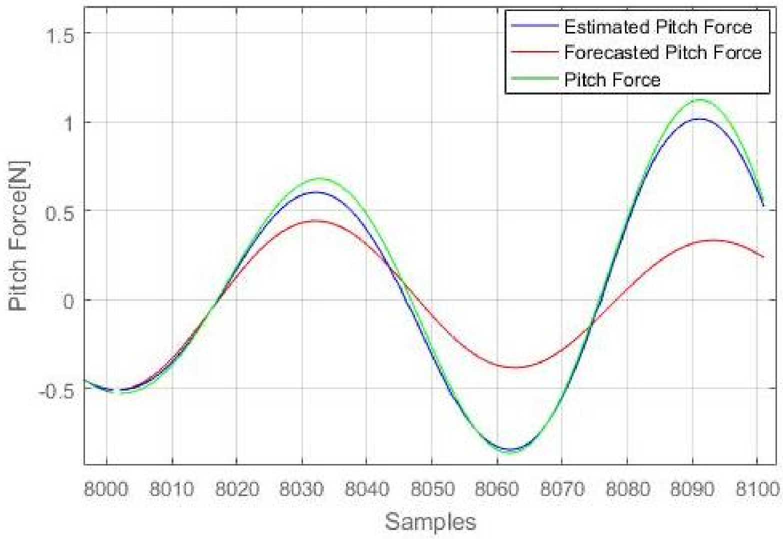

Figure 4.13: Prediction on Data Set 46

In figure 4.13 it is shown the comparison between the Pitch Force simulated by the first-principles based simulator, which inputs belong to Data Set 46, the estimated Pitch Force by the Virtual Sensor and the forecasted Pitch Force. Along the prediction horizon the value of the GoF index between the forcasted output and the estimated one is 42.56%, while between the forecasted and the simulated is 40.54%.The prediction improves in the first 2s with a fitting of 93.7% with the estimated Pitch Force and 90% with the simulated.

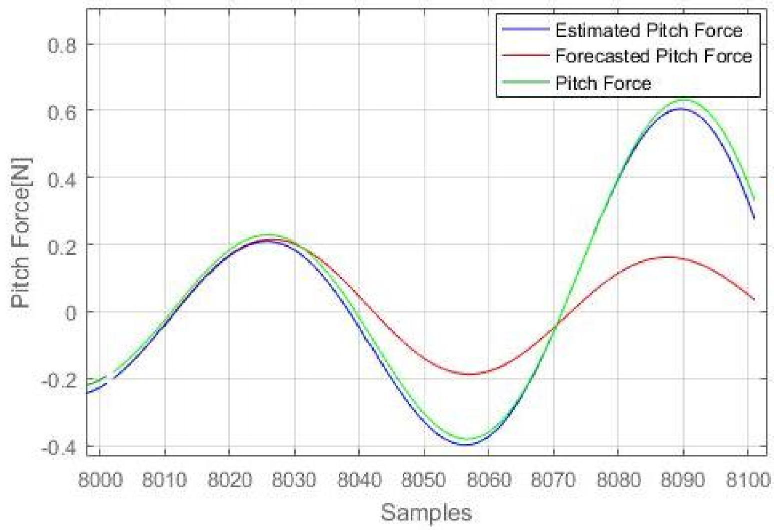

Figure 4.14: Prediction on Data Set 48

In figure 4.14 it is shown the comparison between the Pitch Force simulated by the first-principles based simulator, which inputs belong to Data Set 48, the estimated Pitch Force by the Virtual Sensor and the forecasted Pitch Force. Along the prediction horizon the value of the GoF index between the forcasted output and the estimated one is 32.85%, while between the forecasted and the simulated is 32%.The prediction improves in the first 3s with a fitting of 95.5% with the estimated Pitch Force and 91.3% with the simulated.

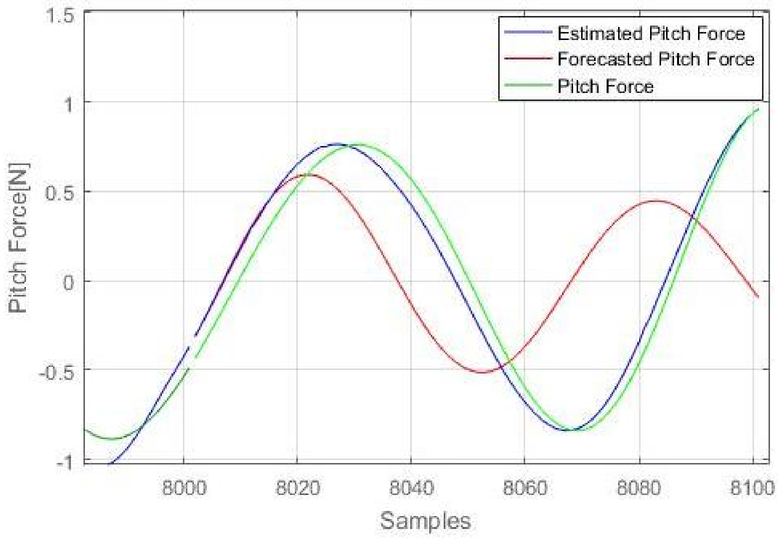

Figure 4.15: Prediction on Data Set 86

In figure 4.15 it is shown the comparison between the Pitch Force simulated by the first-principles based simulator, which inputs belong to Data Set 86, the estimated Pitch Force by the Virtual Sensor and the forecasted Pitch Force. Along the prediction horizon the value of the GoF index between the forcasted output and the estimated one is 9.33%, while between the forecasted and the simulated is 0.01%.The prediction improves in the first 2s with a fitting of 92% with the estimated Pitch Force and 56.9% with the simulated.

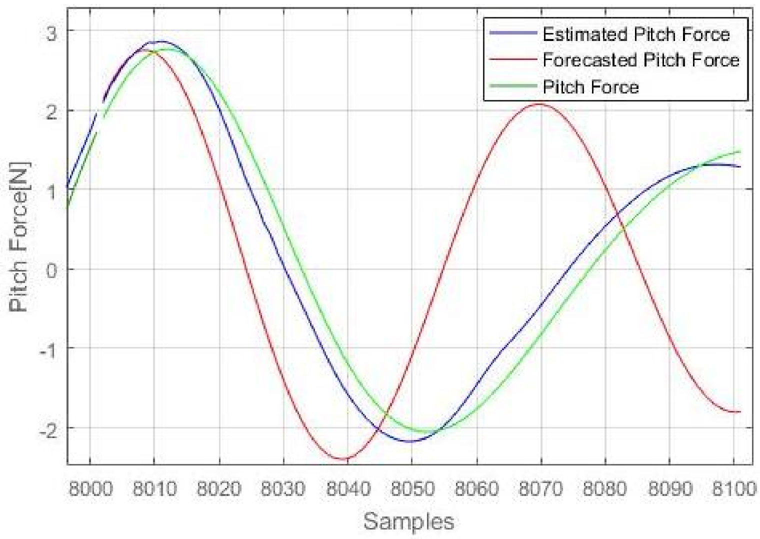

Figure 4.16: Prediction on Data Set 125

In figure 4.16 it is shown the comparison between the Pitch Force simulated by the first-principles based simulator, which inputs belong to Data Set 125, the estimated Pitch Force by the Virtual Sensor and the forecasted Pitch Force. Along the prediction horizon the value of the GoF index between the forcasted output and the estimated one is -4.24%, while between the forecasted and the simulated is -16.6%.The prediction improves in the first 1.5s with a fitting of 89.8% with the estimated Pitch Force and 88% with the simulated.

4.1.3 Comparison Between The Two Predictors

The results previously obtained are summarized in the following tables:

Order 200			
Data Set	**Time(s)**	GoF_e	GoF_s
84	6	82.9%	78.8%
06	2	82.97%	76.3%
08	2	80.9%	79.7%
44	-	-	-
46	1.5	85.8%	87.9%
48	0.5	84%	72.5%
86	3	93.9%	80.9%
125	4	93%	78.5%

Order 10			
Data Set	**Time(s)**	GoF_e	GoF_s
84	3	89%	77.7%
06	2	94%	84.6%
08	2	77%	75.5%
44	$4-7$	63%	90%
46	2	93.7%	90%
48	3	95.5%	91.3%
86	2	92%	56.9%
125	1.5	89.8%	88%

GoF_e is the Goodness of Fit index between the forcasted output and the estimated one, GoF_s is the Goodness of Fit index between the forcasted and the simulated. Looking at the table above, it is possible to notice that:

- Data Set 44 is the one which generates worse results, both in Identification and Prediction. With a predictor of order 200 it is not possible to predict the Pitch Force on this Data Set while with the predictor of order 10 the behaviour is particular: the prediction is accurate but only in the interval between 4s and 7s.
- The prediction horizon with the predictor of order 200 is longer, 6s (on Data Set 84) and 4s (on Data Set 125) against the 3s (on Data Set 84 and 48) with the 10^{th} order predictor.
- The 10^{th} order predictor is not able to provide a good prediction on Data Set 86, while the 200^{th} predictor does not provide a good prediction on Data Set 48 (prediction horizon of 0.5s).
- The fitting is higher for the 10^{th} order predictor, in this case $GoF_{s,max} = 91.3\%$ while for the 200^{th} order system $GoF_{s,max} = 87.9\%$.

Chapter 5

Conclusion

As explained above, this thesis has been conceived with the aim of simplifying the previous study about the prediction algorithm for the ISWEC system, which is composed of a virtual sensor and an autoregressive predictor but in this case the virtual sensor is designed by means of a neural network. This approach has been developed in [5] and it is briefly summarized and discussed in this chapter.

5.1 Neural Network Approach

The informations here contained are derived from [5].
The advantage of a feedforward neural network is that varying the parameters and the order of the neural network it is possible to approximate whichever function. Considering that the relationship between the measurements provided by the on board sensors and the pitch force is nonlinear, the Virtual Sensor can be designed through a single layer feedforward network formed by three layers:

- Input layer
- Hidden layer
- Output layer

they are respectively used for data acquisition, data processing and computation of the network's output.

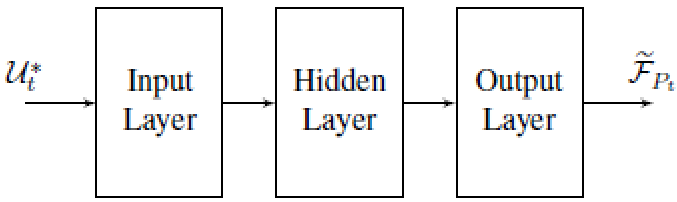

Figure 5.1: Feedforward Neural Network Layers

Training the network consists in optimizing its parameters (weights and biases) given a set of input and output data and an algorithm which works according to the performance goal that in this case is minimize the Mean Squared Error:

$$MSE = \frac{1}{N}\sum_{j=1}^{N}(F_P(i) - \tilde{F_P}(i))^2 \tag{5.1}$$

where N is the number of samples in the data set.
Seven data sets, generated by the simulator and describing seven admissible sea wave conditions, have been used to design the virtual sensor. Only a portion of each data set has been used for the design,

the remaining has been used for validating the designed virtual sensor.
Knowing the measurements coming from the virtual sensor, it is now possible to design an autoregressive predictor of order n which is chosen as the trade off between model's complexity and accuracy. The accuracy is defined by the Goodness-of-Fit criteria:

$$GoF = 1 - \sqrt{\frac{\sum_{i=1}^{N}(\widehat{F}_P(t+i) - \widehat{F}_{P*}(t))^2}{\sum_{i=1}^{N}(\widehat{F}(t+i))^2}} \tag{5.2}$$

where

$$\widehat{F}(t) = \sum_{j=1}^{n_p} a_j \widehat{F}(t-j) \tag{5.3}$$

where a_j are the parameters of the AR predictor. Regarding the predictor's order the best trade off between complexity and accuracy is $n_p = 20$.

5.1.1 Results and considerations

In the following table is shown the performance of the Virtual Sensor in terms of Goodness-of-Fit index for seven validation data sets.

Data Set	**GoF**
01	98%
02	97.68%
03	98.35%
04	98.17%
05	97.96%
06	98.5%
07	98.73%

Table 5.1: Virtual Sensor Performance

For each data set exists a neural network able to accurately estimate in real time the Pitch Force, with a GoF index grater than 97%. Regarding the Autoregressive Predictor, the GoF index is grater than 90% and the prediction is accurate over an horizon of 10s [5].

The drawback of this approach is its complexity since for the virtual sensor a different neural network is needed for each data set. This is the starting point of this thesis, looking for an algorithm more robust. The Set Membership approach leads to a worse accuracy and prediction capability, as shown in chapters 3 and 4, but from the implementation point of view the solution shown in this document is simpler and more robust with respect to the different experimental conditions.

Bibliography

[1] https://ec.europa.eu/eurostat/statistics-explained/index.php?title=Renewable_energy_statistics/it&oldid=401184

[2] G. Vissio and G. Mattiazzo, ISWEC toward the sea - Development, Optimization and Testing of the Device Control Architecture. PhD thesis, 2017.

[3] R.Novo, A Harmonic Balance simulation framework for the ISWEC wave energy device, 2017.

[4] G. Bracco, A. Cagninei, E. Giorcelli, G. Mattiazzo, D. Poggi, and M. Raffero, "Experimental validation of the iswec wave to pto model," Ocean Engineering, vol. 120, pp. 40 – 51, 2016.

[5] V. Cerone, D. Regruto, T. Abdalla, G. Mattiazzo, A Pitch Wave Force Prediction Algorithm for the Inertial Sea Wave Energy Converter